Distinguishing Pseudotransduction and True Transduction Enables Characterization and Bioengineering of Extracellular Vesicle-Adeno-Associated Virus Vectors

Jonathan D. Boucher[1,2,3], Devin M. Stranford[1,3,4], Hailey I. Edelstein[1,3,4], Danielle Tullman-Ercek[1-3,5], Neha P. Kamat[3,5,6], Joshua N. Leonard[1-5,7*]

[1] Department of Chemical and Biological Engineering, Northwestern University, Evanston, Illinois 60208, United States

[2] Interdisciplinary Biological Sciences Program, Northwestern University, Evanston, Illinois 60208, United States

[3] Center for Synthetic Biology, Northwestern University, Evanston, Illinois 60208, United States

[4] Syenex Inc, Evanston, Illinois 60201, United States

[5] Chemistry of Life Processes Institute, Northwestern University, Evanston, Illinois 60208, United States

[6] Department of Biomedical Engineering, Northwestern University, Evanston, IL, 60208 USA

[7] Member, Robert H. Lurie Comprehensive Cancer Center, Northwestern University, Evanston, Illinois 60208, United States

Contact Information

*Corresponding author: Joshua N. Leonard, j-leonard@northwestern.edu

ABSTRACT

Adeno-associated virus (AAV) gene therapies have achieved some clinical success, with multiple products reaching regulatory approval. Encapsulation of AAV vectors within engineered extracellular vesicles (EVs) is an emerging strategy which could help overcome challenges including pre-existing anti-capsid immunity and the need for controlling targeting and tropism. To guide the development of EV-AAV technologies, we developed an assay for quantifying and controlling for the contribution of pseudotransduction to evaluations of EV-AAV-mediated transduction. We developed an AAV vector that switches its transgene output from one reporter to another when acted upon by Cre recombinase expressed in a recipient cell. Using this platform, we investigated EV-AAV transduction as a function of various engineered EV surface modifications. For actively endocytic cells (HEK293FTs), modifications that enhance EV uptake and membrane fusion influence pseudotransduction but not true transduction. Conversely, in less endocytic Jurkat T cells, modifications enhancing EV uptake enhanced both pseudotransduction and true transduction. These conclusions held across two AAV serotypes. Our results provide new insight into prior reports and suggest that effects of enhancing uptake and membrane fusion of EV-AAV vectors are recipient cell type-specific. The methods developed here unambiguously dissect EV-AAV transduction mechanisms and can guide future bioengineering of EV-AAV vectors.

INTRODUCTION

Adeno-associated virus (AAV) gene therapies have substantial promise for the treatment of genetic diseases. Over the last decade, at least seven AAV-based gene therapies have been approved by the US Food and Drug Administration, with hundreds of clinical trials ongoing.[1] Current efforts focus on challenges such as evading preexisting humoral immunity[2], and reducing off-target tissue transduction[3], which both necessitate higher vector doses that are associated with adverse effects[4,5]. One potential strategy for addressing these needs is encapsulation of AAV within engineered extracellular vesicles (EVs).

EVs are nanoscale, membrane-bound particles secreted by all cells and include exosomes, microvesicles, and particles such as apoptotic bodies.[6] Exosomes are formed through the invagination of endosomal compartments, resulting in multivesicular bodies that fuse with the plasma membrane to release exosomes into the extracellular space. These vesicles protect their cargo—cytoplasmic RNA, proteins, and

51 other biomolecules—from degradation by nucleases and proteases.[7] Microvesicles bud from the cell
52 surface and encapsulate a distinct set of biomolecules.[6] When recipient cells take up EVs, some cargo
53 molecules can be released into the cytoplasm to impact cell state.[8,9] Because EVs mediate intercellular
54 communication, exhibit lower toxicity and immunogenicity than synthetic delivery vehicles, and have longer
55 circulation times *in vivo*, they are attractive candidates for therapeutic cargo delivery.[10-12]

56 An interesting observation is that when AAV particles are assembled in producer cells, secreted
57 EVs can incorporate AAV particles capable of conferring gene expression in recipient cells, and such EV-
58 AAV vehicles have distinct properties that are useful for gene delivery.[13] EV-AAVs can mediate transduction
59 of the mouse brain, even when using serotypes not generally able to cross the blood-brain barrier.[14] EV-
60 AAV1 and EV-AAV9 outperformed their free AAV (standard, non-enveloped AAV particle) counterparts in
61 transduction of cochlear hair cells in explant cultures.[15] EV-AAV1 encoding *Lhfpl5,* a protein required for
62 mechanotransduction in outer and inner hair cells and for which loss leads to profound deafness, improved
63 hearing and movement abnormalities in *Lhfpl5*$^{-/-}$ mice.[15] Upon intravitreal injection, EV-AAV2 outperformed
64 free AAV2 in retinal transduction via delivery of GFP, increasing transduction of cell types that are
65 transduced by free AAV2 as well as increasing the extent of transduction across different regions of the
66 retina.[16] EV-AAV8 encoding hF.IX enhanced correction of hemophilia B phenotypes compared to standard
67 AAV8 vectors in C57BL/6 *F9−/−* mice, demonstrating enhanced liver targeting after intravenous injection.[17]
68 Both standard AAV8 and EV-AAV8 can transduce a variety of immune cell populations, including CD4^{+} T
69 cells, CD8^{+} T cells, B cells, macrophages, and dendritic cells after systemic delivery in mice.[18] EV-AAV8
70 can mediate the expression of human interleukin-2 receptor alpha chain (IL-2Rα) in multiple lymphocyte
71 populations, suggesting that EV-AAVs could be utilized for *in vivo* cell engineering.[18] In a lung cancer
72 xenograft mouse model, local injection of EV-AAV6 was much more potent in transducing tumor cells
73 compared to free AAV6.[19] Upon intratracheal injection in C57BL/6 mice, EV-AAV6 enhanced transduction
74 of the lung compared to either free AAV6 or a mixture of free AAV6 and EVs, demonstrating that the
75 enhanced lung transduction by EV-AAV6 was attributable to the direct association of EVs and AAV6.[20] EV-
76 AAV9 delivering *SERCA2a* significantly improved cardiac function in a mouse model of myocardial
77 infarction compared to free AAV9.[21] In addition to improving transduction, EV-AAVs resist neutralization by
78 AAV specific antibodies, suggesting that encapsulation can help address needs for AAV vector

79 delivery.[14,17,19-25] Moreover, since EVs have been engineered to target specific cell types[26-29], it is possible
80 that such methods could target EV-AAVs as well.

81 Although EV-AAV vectors are promising, they are still in the early stages of development as a
82 therapeutic platform. EV-AAVs have been analyzed in pre-clinical models but have yet to be evaluated in
83 human clinical trials. Several key mechanistic questions about EV-AAVs are incompletely understood. First,
84 the functional consequences of surface-functionalizing EV-AAV vectors on recipient cell binding and particle
85 uptake are unclear. Second, reports conflict as to how increasing EV-endosomal fusion modulates
86 transduction by EV-AAV. An early study suggested that functionalizing EV-AAVs by incorporating the low
87 pH-activated fusogen vesicular stomatitis virus glycoprotein (VSV-G) on the EV surface can diminish
88 transduction of HEK293T and U87 glioma cells by AAV2, compared to EV-AAV2 lacking VSV-G.[13] This is
89 surprising as increasing uptake (via VSV-G binding to its receptor, low density lipoprotein receptor, LDL-
90 R[30]) and fusion-mediated entry of the AAV capsid into the cytosol may be expected to increase transduction.
91 While a possible explanation is that AAV2 requires processing in the endosome—capsid cleavage by the
92 endosomal cysteine proteases cathepsins B and L[31], autoproteolytic processing of the capsid at low
93 pH[32], and exposure of the VP1/2 N-terminal region exposing a phospholipase A2 domain that helps the
94 virion escape the endosome and traffic to the nucleus[33,34]—that mechanism is untested in EV-AAV delivery.
95 VSV-G display on EV-AAV2 showed no effect on transduction of several other glioma cell lines compared
96 to non-targeted EV-AAV2[13], suggesting the role of VSV-G may vary by recipient cell type. A related line of
97 evidence is that display of rabies virus glycoprotein (RVG) on the surface of EV-AAV9 increased
98 transduction of SH-SY5Y cells and transduction of the brain of mice compared to non-targeted EV-AAV9.[22]
99 RVG binds to the nicotinic acetylcholine receptor (nAChR), neural cell adhesion molecule (NCAM), p75
100 neurotrophin receptor, integrin β1, and transferrin receptor 1 (TfR1), promoting clathrin-mediated
101 endocytosis of the particle.[35] Much like VSV-G, upon encountering the low pH of the endosome, RVG
102 undergoes conformational changes that promote endosomal membrane fusion and escape.[36,37] Given the
103 similarity in mechanisms used by VSV-G and RVG, the differences in transduction when displayed on EV-
104 AAVs is surprising and may indicate recipient cell type and/or AAV serotype-specific effects. A further
105 consideration is that AAV particles are found on both the surface and interior of EV-AAV particles, adding
106 nuance to the interpretation of these delivery phenomena.[15,17,23] By some estimates, in EV-AAV

107 preparations, approximately 1-2% of EVs may incorporate AAVs.[38] Taken together, EV-AAV preparations
108 are a heterogenous mixture of EVs and EV-AAVs. Although EV-AAV vectors are promising, successful
109 bioengineering of such vectors would benefit from mechanistic understanding of delivery mechanisms.

110 A key technical challenge when evaluating engineered EV-AAV-mediated delivery is distinguishing
111 delivery of protein and/or mRNA originating from transgene expression in producer cells (i.e.,
112 "pseudotransduction"), from gene delivery to and resulting transgene expression in recipient cells.
113 Pseudotransduction is also observed with lentiviral and retroviral vectors, which are also enveloped and
114 can incorporate cytosolic proteins from producer cells.[39-42] In certain applications, pseudotransduction may
115 be useful, as demonstrated in dendritic cell–targeted lentiviral vectors for vaccination, in which incorporated
116 protein antigens are employed to train induced immune reactions.[43] However, in applications where
117 quantification of gene delivery or transduction is desired, pseudotransduction can inflate the rates of
118 transduction reported. Informed in part by prior observations that protein delivery can complicate evaluation
119 of EV-mediated mRNA delivery[44,45], we hypothesized that controlling for pseudotransduction may be
120 particularly crucial for measuring EV-AAV transduction because achieving comparable rates of transduction
121 typically requires higher numbers of particles for EV-AAV compared to lentiviral vectors. Thus,
122 distinguishing transduction from pseudotransduction is critical for the engineering and evaluation of EV-
123 AAV vectors.

124 In this study, we developed and validated a quantitative assay for disambiguating
125 pseudotransduction from transduction by EV-AAVs and applied this method to investigate several biological
126 hypotheses that inform bioengineering. Our assay comprises a modified stoplight system, in which Cre
127 recombinase is expressed in recipient cells where it can modify an incoming engineered AAV vector to shift
128 its transgene expression from one fluorescent protein to another. Using this approach, true transduction
129 (hereafter, simply "transduction") can be distinguished from pseudotransduction. With this system, we
130 compared various EV surface functionalization strategies that drive uptake and/or membrane fusion with
131 recipient cells and determined how these engineering choices impact pseudotransduction and transduction.
132 Such analysis revealed new insights about EV-AAV transduction that would otherwise be obscured by
133 pseudotransduction. Our assay enables generation and testing of new mechanistic hypotheses for studying
134 EV-AAV biology and bioengineering these vectors.

135

136 **METHODS**

137

138 ***General DNA assembly***

139 Plasmids were constructed using standard molecular biology techniques. Plasmid assembly was performed
140 via restriction enzyme cloning. Plasmids were transformed into TOP10 competent Escherichia coli (Thermo
141 Fisher) and grown at 37 °C. AAV vector (transfer) plasmids were transformed into NEB Stable competent
142 Escherichia coli (New England Biolabs C3040) and grown at 37 °C. Plasmid cloning was performed
143 primarily using standard restriction enzyme cloning with restriction enzymes (NEB), T4 DNA Ligase (NEB
144 M0202L), and Antarctic Phosphatase (NEB M0289L). Plasmids with pcDNA-based backbones were
145 transformed into chemically competent TOP10 *Escherichia coli* (Thermo Fisher C404010), and cells were
146 grown at 37°C. Plasmids with AAV transgene vector backbones were transformed into chemically
147 competent NEB Stable *Escherichia coli* (NEB C3040H), and cells were grown at 30°C.

148

149 ***Source vectors for DNA assembly***

150 The AAV transfer vector (pAAV-GFP SN), and helper plasmid (pHelper) were gifts from David Schaffer
151 (University of California, Berkeley). The LumiScarlet gene was PCR amplified from pcDNA3-LumiScarlet,
152 which was a gift from Huiwang Ai (Addgene plasmid # 126623 ; http://n2t.net/addgene:126623 ;
153 RRID:Addgene_126623)[46], and cloned into the pAAVGFP SN plasmid using AgeI and NotI. pOTTC1032 -
154 pAAV EF1a Nuc-flox(mCherry)-EGFP (pJB037) was a gift from Brandon Harvey (Addgene plasmid #
155 112677 ; http://n2t.net/addgene:112677 ; RRID:Addgene_112677).[47] Gene strings for the other Cre-
156 responsive vectors (pJB038 - No NLS and eGFP, pJB040 - NLS and mNeonGreen, and pJB041 No NLS
157 and mNeonGreen) were codon optimized and synthesized by ThermoFisher (GeneArt), then cloned into
158 the pOCTTC1032 plasmid using KpnI and EcoRI restriction enzymes. RepCap plasmids for AAV2
159 (pRep2Cap2) and AAV6 (pRep2Cap6) were gifts from the Vector Core at the University of Pennsylvania
160 (Penn Vector Core (RRID: SCR_022432)). pcDNA is plasmid pPD005 (Addgene plasmid # 138749 ;
161 http://n2t.net/addgene:138749 ; RRID:Addgene_138749).[48] psPAX2 and pMD2.G plasmids were gifted by
162 William Miller from Northwestern University. pHIE822 was created by introducing point mutations (K47Q,

163 R354A) in the VSV-G-encoding gene of pMD2.G using site-directed mutagenesis by PCR. pCMV-VSV-
164 G(P127D)-Myc (pJB042) was a gift from Wesley Sundquist (Addgene plasmid # 80055 ;
165 http://n2t.net/addgene:80055 ; RRID:Addgene_80055).[49] pHIE963 was created using standard restriction
166 enzyme cloning to insert a Cre recombinase gene into a third-generation lentiviral transfer vector provided
167 by Twist Bioscience (pTwist Lenti SFFV PuroR). The Cre recombinase gene was amplified by PCR from
168 pBS185 CMV-Cre, which was a gift from Brian Sauer (Addgene plasmid # 11916
169 ; http://n2t.net/addgene:11916 ; RRID:Addgene_11916).[50] The Ultra-HEK plasmid is a commercial product
170 made by Syenex. The plasmids used to produce Ultra-HEK lentiviral vectors are Syenex plasmids: SNX-
171 mNG-TV3, SNX-Gagpol, SNX-Rev, and SNX-VSV-G. A list of plasmids utilized in this study can be found
172 in **Supplementary Data 1**. Plasmid sequences can be found in **Supplementary Data 2**.
173
174 ***Plasmid preparation***
175 TOP10 or NEB Stable *E. coli* were grown overnight, shaking at 37°C or 30°C, respectively, in 50-100 mL of
176 LB media with the appropriate selective antibiotic. The next day, DNA was prepped using a ZymoPURE II
177 Plasmid Midiprep Kit (Zymo D4201) following the manufacturer's instructions. DNA purity and
178 concentrations for relevant experiments were measured with a NanoDrop 2000 (Thermo Fisher Scientific).
179 All plasmid sequences were confirmed by whole plasmid sequencing, including AAV transfer plasmids to
180 ensure ITR integrity.
181
182 ***Cell culture***
183 FreeStyle 293-F cells (Gibco R79007) cells were cultured in FreeStyle 293 Expression Medium (Gibco
184 12338018) supplemented with 1% penicillin–streptomycin (Gibco 15140-122). HEK293FT cells (Thermo
185 Fisher R70007) were cultured in Dulbecco's modified Eagle medium (DMEM, Gibco 31600-091)
186 supplemented with 10% fetal bovine serum (FBS) (Gibco 16140-071), 1% penicillin–streptomycin (Gibco
187 15140-122) and 4 mM additional L-glutamine (Gibco 25030-081). HEK293T Lenti-X cells (Takara 632180)
188 were cultured in HEK293FT media formulation supplemented with 1 mm sodium pyruvate from Gibco
189 (11360070). Jurkat T cells (ATCC TIB-152) were cultured in Roswell Park Memorial Institute medium (RPMI
190 1640, Gibco 31800-105) supplemented with 10% FBS, 1% penicillin–streptomycin, and 4 mM L-glutamine.

191 Sublines generated from these cell lines were cultured in the same way. Cells were subcultured at a 1:5 or
192 1:10 ratio every 2–3 days, using trypsin–EDTA (Gibco 25300-054) to remove adherent cells from the plate.
193 Freestyle 293-F cells were maintained at 37 °C with 8% CO_2 rotating at 135 rpm on a shaking platform
194 (Infors HT Multitron – I8000A) with orbital diameter 25 mm. HEK293FT, HEK293T Lenti-X, and Jurkat cells
195 were maintained at 37 °C with 5% CO_2. Freestyle 293F, HEK293FT, HEK293T Lenti-X and Jurkat cells
196 tested negative for mycoplasma with the MycoAlert Mycoplasma Detection Kit (Lonza LT07-318).
197
198 ***Cell line generation***
199 To generate lentivirus, HEK293T Lenti-X cells were plated in 10 cm dishes at a density of 5×10^6 cells per
200 dish (6.25×10^5 cells per ml). About 24 h later for Lenti-X, cells were transfected with 10 µg of lentiviral
201 transfer vector plasmid, 8 µg of psPAX2 second generation lentiviral packaging plasmid, and 3 µg pMD2.G
202 VSV-G-encoding plasmid via calcium phosphate transfection. Briefly, DNA was diluted with sterile H_2O and
203 added to $CaCl_2$ (2 M) to achieve a final concentration of 0.3 M $CaCl_2$. DNA-containing samples were then
204 added dropwise to an equal-volume of 2X HEPES-buffered saline (280 mM NaCl, 0.5 M HEPES, 1.5 mM
205 Na_2HPO_4) and pipetted four times to mix. After 3–4 min, the solution was vigorously pipetted eight times
206 and 2 mL of transfection reagent per 10 cm dish was added dropwise to cells. The plates were gently swirled
207 and incubated overnight at 37°C with 5% CO_2. The medium was replaced the morning after transfection
208 and cells were incubated for an additional 28–30 h. At 28 h post-medium change, lentivirus was collected
209 from the conditioned medium. The medium was centrifuged at 500 x *g* for 2 min to clear cells, and the
210 supernatant was filtered through a 0.45 µm PES pore filter (VWR). Lentivirus was concentrated from the
211 filtered supernatant by ultracentrifugation in Ultra Clear tubes (Beckman Coulter 344059) at 100,420 x *g* at
212 4 °C in a Beckman Coulter Optima L-80 XP ultracentrifuge using an SW41Ti rotor. The supernatant was
213 aspirated, leaving virus in ~100 µl final volume (~100X concentration), and concentrated lentivirus was left
214 on ice for at least 30 min before resuspension, then used to transduce $\sim 1 \times 10^5$ cells, plated either at the
215 time of transduction or on the day before. When appropriate, drug selection began 2 d post transduction,
216 using antibiotic concentrations of 1 µg ml^{-1} puromycin (Invitrogen ant-pr) on HEK293FT cells or 0.2 µg ml^{-1}
217 puromycin on Jurkat cells. Cells were kept in antibiotics for at least 2 weeks with subculturing every 1–2 d.
218

219 ***Transfection***

220 For transfection of Freestyle 293-F cells, a transfection protocol previously used to make AAV from
221 suspension HEK cells was utilized.[51] Briefly, 3 d before transfection cells were plated in fresh FreeStyle 293
222 Expression Medium at a concentration of 1×10^6 cells per mL. On the day of transfection, Freestyle 293-F
223 cells were spun at 150g x 5 min and resuspended in fresh FreeStyle 293 Expression Medium. The cells
224 were counted and plated at a density of 1×10^6 cells per mL. Cells were transfected with 1.5 µg of DNA per
225 million cells by PEI transfection. Plasmid DNA was added to a volume of room temperature (~20°C)
226 FreeStyle 293 Expression Medium, corresponding to 5% of the total volume in the flask to be transfected.
227 The tube was mixed to evenly distribute plasmid DNA. 3 µg of PEI (Polysciences, Inc – 24765) per million
228 cells was added to the tube and vortexed. The tube was then incubated for 10 min at room temperature to
229 allow for precomplex formation and then added directly to the flask.

230

231 ***EV-AAV production, isolation, and concentration***

232 Freestyle 293-F producer cell lines were transfected as described in Transfection. For EV-AAVs, the AAV
233 vector plasmid (transfer), packaging plasmid (rep/cap), and adenoviral helper plasmid (pHelper) were
234 transfected in equal DNA mass ratios up to the maximum DNA amount for the mixture. In transfections used
235 to make EV-AAV vectors including two types of EV surface protein, the mass ratio of transfected plasmids
236 was 1:1:1:1.59:1.41 for the AAV vector plasmid (transfer), packaging plasmid (rep/cap), adenoviral helper
237 plasmid (pHelper), pMD2.G VSV-G plasmid, and Ultra-HEK plasmid respectively. For control vectors in
238 which one such EV surface protein was omitted, pcDNA was included instead (at the equivalent DNA mass)
239 to ensure the same total mass of DNA was transfected into each flask. In experiments comparing various
240 single EV surface functionalizations, an equivalent mass of plasmid encoding each surface protein was
241 used, with the remaining mass made up by the AAV vector plasmid (transfer), packaging plasmid (rep/cap),
242 adenoviral helper plasmid (pHelper) at equivalent mass ratios. For exact DNA doses, see **Supplementary**
243 **Data 3**. 3 d after transfection, EV-AAVs were collected from the conditioned medium by differential
244 centrifugation. Briefly, conditioned medium was cleared of debris by centrifugation at 300 x g for 10 min to
245 remove cells followed by centrifugation at 2,000 x g for 20 min to remove dead cells and apoptotic bodies
246 in a Sorvall Legend X1R Centrifuge (ThermoFisher Scientific 75004261) with a TX-400 4 x 400 mL Swinging

247 Bucket Rotor. All centrifugation steps were performed at 4 °C. The supernatant underwent tangential flow
248 filtration using a KrossFlo KR2i TFF System with a MICROKROS 20CM 500KD filter (Repligen C02-S500-
249 05-S). Supernatant was flowed through the system at 24.99 mL/min at a constant transmembrane pressure
250 of 6.0 psi. The supernatant was concentrated to approximately 5 mL by TFF. In between samples, the TFF
251 was cleaned with at least 50 mL of 0.2 M NaOH that was sterile filtered by a 0.22 μm bottle top filter (Corning
252 431118). The system was then washed with at least 100 mL of PBS filtered by a 0.1 μm bottle top filter
253 (Corning 431475). The TFF system was kept in 0.05% sodium azide (EMD SX0299-1) in H_2O to prevent
254 contamination. After TFF, the EV-AAVs were further concentrated to approximately 0.5 mL (~800X
255 concentration) in Amicon Ultra-4 100K Centrifugal Filters (Millipore UFC810024) that were pre-washed with
256 0.1 μm bottle top filtered PBS. 0.5 mL of concentrated EV-AAVs were treated with Benzonase (25 U/mL,
257 EMD Millipore 70664) supplemented with $MgCl_2$ at a concentration of 2 mM for 1 h at 37 °C. Samples were
258 then purified to remove free AAV and other non-EV proteins using one of the methods below.
259
260 ***EV iodixanol purification***
261 Iodixanol gradient purification of EVs was modified from a previous report.[21] Briefly, 1x PBS-MK buffer was
262 prepared by dissolving 26.3 mg of MgCl2 and 14.91 mg of KCl in 100 mL of 1x PBS. The solution was
263 sterilized by passing it through a 0.22 μm filter (Corning 431118). 1 M NaCl/PBS-MK buffer was prepared
264 by dissolving 5.84 g of NaCl, 26.3 mg of MgCl2 and 14.91 mg of KCl in 1X PBS in a final volume of 100
265 mL. The solution was sterilized by passing it through a 0.22 μm filter (Corning 431118). Three iodixanol
266 (Sigma Alrich D1556) gradients were prepared from these solutions: 25% iodixanol (5 mL of 60% iodixanol,
267 7 mL of 1x PBS-MK buffer), 40% iodixanol (6.7 mL of 60% iodixanol and 3.3 mL of 1x PBS-MK buffer) and
268 60% iodixanol (10 mL of 60% iodixanol). These solutions were layered into UltraClear tubes (Beckman
269 Coulter 344059) in the following order: 1 mL 60% iodixanol, 3 mL 40% iodixanol, and 5 mL 25% iodixanol.
270 EVs were layered on top of the 25% iodixanol layer. The tubes were spun in a Beckman Coulter Optima L-
271 80 XP ultracentrifuge with an SW41 Ti rotor at 190,000 x g for 3 h at 18°C. After the spin, EVs were visible
272 as a white band in the 25% layer and were removed with a syringe with 18G needle. To remove the iodixanol
273 from the EVs, EVs were placed in a new UltraClear tube and diluted in PBS. The tubes were spun at
274 120,000 x g for 90 min at 4 °C to pellet the EVs. After the spin, the supernatant was aspirated, and EV

275 pellets were left in ~100–200 µl of PBS. EVs were incubated on ice for at least 30 min after supernatant
276 removal before resuspension in a total of 500 µL of PBS.
277
278 ***EV size exclusion chromatography purification***
279 Size exclusion chromatography was performed using qEVoriginal (35 nm) Gen2 columns (Izon ICO-35)
280 attached to an Automatic Fraction Collector V1 (Izon). We followed the manufacturer's instructions by
281 equilibrating the SEC column in PBS sterilized with 0.1 µM bottle top filters (Corning 431475). 0.5 mL of
282 EVs were placed on the column and EV fractions 1-4 were collected based on the manufacturer's
283 instructions and a previous report of EV-AAV purification with these SEC columns[25]. Fractions 1-4 were
284 combined and concentrated to approximately 250 µL in Amicon Ultra-4 100K Centrifugal Filters (Millipore
285 UFC810024) that were pre-washed with 0.1 µm bottle top filtered PBS.
286
287 ***EV concentration determination by Nanoparticle Tracking Analysis (NTA)***
288 EV concentration was determined by NanoSight analysis. Samples were diluted in PBS sterilized with 0.1
289 µM bottle top filters (Corning 431475) to concentrations on the order of 10^8 particles per ml for analysis.
290 NanoSight analysis was performed on an NS300 (Malvern), software version 3.4. Three 30 s videos were
291 acquired per sample using a 642 nm laser on a camera level of 14, an infusion rate of 30 and a detection
292 threshold of 7. Default settings were used for the blur, minimum track length and minimum expected particle
293 size. EV concentrations were defined as the mean of the concentrations calculated from each video. Size
294 distributions were generated by the software.
295
296 ***AAV crude cell lysate production***
297 AAV was harvested from the Freestyle 293-F cell lysates of cells transfected to make non-targeted EV-
298 AAVs (no EV surface modifications). Briefly, 72 h post-transfection the EV-AAV containing supernatant was
299 removed and the cells were resuspended and washed with PBS sterilized with 0.1 µM bottle top filters
300 (Corning 431475). The cells were spun at 1000 x g for 7 min in a Sorvall Legend X1R Centrifuge
301 (ThermoFisher Scientific 75004261) with a TX-400 4 x 400 mL Swinging Bucket Rotor. The supernatant
302 was removed, and the cells were mixed with AAV lysis buffer corresponding to 2% of the initial culture

303 volume. AAV lysis buffer was made by combining 2 mL of 5 M NaCl, 0.158 g Tris-HCl and H_2O up to 100
304 mL. The solution was pH-adjusted to 8.5 and sterile filtered by a 0.22 µm bottle top filter (Corning 431118).
305 The cell pellet resuspended in AAV lysis buffer was then frozen in a bath of dry ice and ethanol, followed
306 by thawing in a 37°C bead bath. After each thawing the solution was vortexed vigorously for 30 s. The cell
307 pellet underwent three rounds of freeze/thaws. Benzonase (50 U/mL, EMD Millipore 70664) was added to
308 the mixture and incubated for 30 min at 37°C. The solution was transferred to 1.5 mL microcentrifuge tubes
309 and spun at 7000 rpm for 15 min in a microcentrifuge (Eppendorf Centrifuge 5424). The supernatant,
310 clarified AAV crude lysate, was transferred to a clean microcentrifuge tube and stored at 4°C until further
311 processing.
312
313 ***AAV purification by iodixanol gradient centrifugation***
314 1x PBS-MK buffer was prepared by dissolving 26.3 mg of MgCl2 and14.91 mg of KCl in 100 mL of 1x PBS.
315 The solution was sterilized by passing it through a 0.22 µm filter (Corning 431118). 1 M NaCl/PBS-MK buffer
316 was prepared by dissolving 5.84 g of NaCl, 26.3 mg of MgCl2 and 14.91 mg of KCl in 1X PBS in a final
317 volume of 100 mL. The solution was sterilized by passing it through a 0.22 µm filter (Corning 431118). Four
318 iodixanol (Sigma Alrich D1556) gradients were prepared from these solutions: 15% iodixanol (4.5 mL of
319 60% iodixanol and 13.5 mL of 1 M NaCl/PBS-MK buffer), 25% iodixanol (5 mL of 60% iodixanol, 7 mL of 1x
320 PBS-MK buffer and 30 µL of phenol red), 40% iodixanol (6.7 mL of 60% iodixanol and 3.3 mL of 1x PBS-
321 MK buffer) and 60% iodixanol (10 mL of 60% iodixanol and 45 µL of phenol red). These solutions were
322 layered into UltraClear ultracentrifuge tubes (Beckman Coulter 344059) in the following order: 1.35 mL 60%
323 iodixanol, 1.35 mL 40% iodixanol, 1.6 mL 25% iodixanol, 2.7 mL 15% iodixanol, and up to 4 mL of AAV
324 Crude Lysate. The tubes were spun in a Beckman Coulter Optima L-80 XP ultracentrifuge with an SW41 Ti
325 rotor at 190,000 x g for 3 h at 18°C. AAV was removed by inserting a syringe with 18G needle at the border
326 between the 60% and the 40% iodixanol fractions, with the needle facing upward to the lower portion of the
327 40% iodixanol fraction where the viral particles accumulate. The entire 40% iodixanol layer (transparent)
328 was removed without disturbing the layer of protein contaminants that accumulate at the interphase
329 between the 40% and 25% iodixanol layers. To remove the iodixanol this layer was mixed 1:1 by volume
330 with PBS and added to an Amicon Ultra-15 100K spin filter. The spin filter was spun at 3000 x g until the

331 volume remaining in the column was less than 1 mL. PBS was added to the column to the full volume and
332 spun at 3000 x g until 1 mL remained in the column. This was PBS washing was repeated 4 more times to
333 remove iodixanol and concentrate the AAV to its final volume.
334
335 ***AAV purification by magnetic beads***
336 Free AAV was purified using Dynabeads Capture Select AAVX Magnetic Beads (Thermofisher Scientific
337 2853522001) by the manufacturer's protocol. Briefly, 40 µL of bead slurry was added to a low protein binding
338 microcentrifuge tube with 460 µL of PBS. The tubes were placed on a magnetic stand and once the beads
339 were collected on the side of the tube the supernatant was removed. The beads were then mixed with 500
340 µL of PBS, the tubes were placed on a magnetic stand, and the supernatant was removed. 1 mL of AAV
341 crude lysate was added to the beads and the tubes were put on a rotating platform to continuously mix the
342 beads and lysate for 30 min. After 30 min the beads were collected with the magnetic stand and the
343 supernatant was removed. 500 µL of PBS was mixed with the beads, the beads were collected on the
344 magnetic stand, and the supernatant was removed. This PBS wash was repeated again. 20–50 µL of elution
345 buffer was added to the beads and mixed well. The elution buffer (50 mM citric acid, pH 2.5–3.0) and beads
346 were incubated at room temperature for 10 min with occasional pipetting. The beads were collected on the
347 magnetic stand and the supernatant containing purified AAV was collected. The eluted AAV mixture was
348 neutralized by adding 1 µL of Neutralization Buffer (1 M Tris-HCl, pH 8.7) for each 10 µL of eluate.
349
350 ***Physical titer determination by qPCR***
351 First, 5 µL of the EV-AAV, purified AAV, or clarified crude lysate samples were mixed with 39 µL nuclease-
352 free H_2O, 5 µL of 10x DNaseI buffer (ThermoFisher B43) and 1 µL of DNaseI (ThermoFisher EN0521) to
353 eliminate plasmid DNA, incubating at 37°C for 1 h followed by a 15 min inactivation step at 75°C. Samples
354 were placed on ice. Then, viral genomic DNA (vgDNA) was extracted using the High Pure Viral Nucleic Acid
355 Kit (Roche 11858874001), following manufacturer instructions. qPCR analysis was performed by amplifying
356 a sequence within the LumiScarlet reporter using primers CAGGGAGGTTTGACCAGTTT (forward), and
357 GGATATCGATCTTCAGCCCATT (reverse) or the mCherry reporter using the primers
358 AGGACGGCGAGTTCATCTA (forward), and CCCATGGTCTTCTTCTGCATTA (reverse). Primers were

359 designed using IDT's PrimerQuest Tool. A plasmid containing the LumiScarlet transgene (pJB035) or
360 mCherry transgene (pJB040) were used as a standard; serial dilutions were prepared using EASY dilution
361 (Takara Bio 9160), plating each dilution in duplicate. The vgDNA samples were diluted in nuclease free
362 H_2O, plating 4 serial dilutions per sample (in duplicate). For each qPCR reaction (each in a 96-well), 5 µL
363 of vgDNA sample were mixed with 10 µL Universal SYBR Master Mix 2x (ThermoFisher K0221), 0.15 µL
364 of 100 µM forward primer, 0.15 µL of 100 µM reverse primer, and 4.7 µL of nuclease free H_2O. qPCR plates
365 were sealed and spun at 500 x g for 2 min before placing in Bio-Rad C1000 Thermal Cycler with CFX96
366 Real-Time System. Samples run to detect LumiScarlet were heated to 98°C for 3 min, followed by 40 cycles
367 of: 98°C for 15 s, 62°C for 30 s. Then, a final step of 0.5°C increments every 5 s from 65°C to 95°C was
368 performed. Samples run to detect mCherry were heated to 98°C for 3 min, followed by 40 cycles of: 98°C
369 for 15 s, 55°C for 30 s. Then, a final step of 0.5°C increments every 5 s from 65°C to 95°C was performed.
370

371 ***Transduction assays***

372 For most experiments, EV-AAV or free AAV vectors were diluted in 0.1 µm bottle top filtered PBS so that
373 100 µL of the dilution contained 10^9 vector genomes. 100 µL of the diluted vector was added to each well
374 of a 24-well plate. Recipient cells were diluted to 10^4 cells per 900 µL of media and added to the wells with
375 vector, for a final dosage of 10^5 vector genomes per cell. For the experiments depicted in **Figure 4E-F** and
376 **Figure S17E-F**, 2 x 10^9 vector genomes were added per well (2 x 10^5 vector genomes per cell). To provide
377 some rationale, our initial transduction assays (**Figure 4C-D, Figure S17B-C)** yielded fairly low transduction
378 efficiencies, so the dose was increased in subsequent experiments (**Figure 4E-F, Figure S17E-F**). Negative
379 control wells received 100uL of 0.1 µm bottle top filtered PBS. After the addition of all vectors and recipient
380 cells, the plate was vigorously mixed and placed in an incubator. 5 d post transduction, cells were harvested
381 for flow cytometry using 0.05% Trypsin-EDTA with phenol red for HEK293FT recipient cells for 5 min
382 followed by quenching with medium. The resulting cell solution was added to at least 2 volumes of FACS
383 buffer (PBS pH 7.4, 2–5 mM EDTA, 0.1% BSA) supplemented with DAPI (to identify live cells) at a final
384 concentration of 3 µM. Jurkat cells were pipetted from the plate directly into FACS tubes containing FACS
385 buffer supplemented with DAPI. A single FACs tube of PBS treated cells was added to a tube containing
386 FACS buffer without DAPI to identify live cells (DAPI negative). Cells were centrifuged (150 × g for 5 min),

387 supernatant was decanted, fresh FACS buffer, with or without DAPI, was added, and cells were
388 resuspended by briefly vortexing.
389
390 For experiments involving lentiviral transduction of HEK293T and HEK293FT by lentiviral vectors including
391 Ultra-HEK, similar methods were used. Cell lines were harvested, counted, and plated in 96-well, TC
392 treated, PBS-moated, flat-bottom plates at a density of 10^5 cells/mL in a volume of 100 µL per well (10^4
393 cells/well). Crude LV supernatant was diluted 5-fold seven times in complete DMEM to generate a seven-
394 point dilution curve starting from the first dilution. Cells were transduced by adding 100 µL/well of LV (each
395 dilution) and were incubated for 3 d at 37°C. Before analysis of transduction by flow cytometry, cells were
396 harvested by aspirating the media, trypsinizing cells for 5 min at room temperature, quenching with
397 complete DMEM, transferring lifted cells to a non-treated, round-bottom 96-well plate, spinning cells at 150
398 x g for 5 min, and resuspending in 30 µL of FACS buffer (PBS pH 7.4 with 0.05% BSA and 2 mM EDTA) +
399 DRAQ7 viability dye (Thermo Fisher D15106, diluted 1000x). DRAQ7 was used to identify live cells (DRAQ7
400 negative) for analysis.
401
402 ***Microscopy imaging***
403 Microscopy was conducted on a Keyence BZ-X800E fluorescence microscope and a Nikon CFI S Plan
404 Fluor ELWD 20XC objective (MRH08230). LumiScarlet fluorescence was imaged with a Keyence BZ-X
405 Filter TexasRed (Keyence, OP-87765). Images were taken using the Keyence BZ Series Viewer Software
406 (Version 01.03.00.01) in high resolution mode. Scale bars were added to images with the BZ-X800 Analyzer
407 Software (Version 1.1.2.4).
408
409 ***Transfected producer cell analysis***
410 Freestyle 293-F producer cell lines were transfected as described in Transfection. For each condition, 3
411 flasks of 20 x 10^6 cells in 20 mL of Freestyle media were plated. Cells were transfected with 30 µg total of
412 DNA. For each condition and exact DNA doses, see **Supplementary Data 3**. 3 d after transfection, 1 mL
413 of cells and media were removed from each flask, placed in a FACS tube and spun at 150 x g for 5 min.
414 The media was removed, and the cells were washed with PBS. The cells were spun at 150 x g for 5 min

415 and the supernatant was removed. 1 mL of 4% paraformaldehyde in PBS (Thermo Scientific, J61899.AK)
416 was added to each tube, gently vortexed and fixed for 20 min at room temperature. Cells were then washed
417 3 times with 1 mL of PBS. After the final wash, cells were resuspended in FACS buffer and analyzed by
418 flow cytometry.
419
420 ***Cycloheximide (CHX) treatment of recipient cells***
421 1.0 x 10^5 HEK293FT recipient cells per well in 1 mL of DMEM were plated in 24-well plates the night before
422 treatment. Treatments (EV-AAV2, No Rep/Cap EVs, free AAV2) were diluted in 0.1 µm bottle top filtered
423 PBS so that 100 µL of the dilution contained 10^9 vector genomes. No Rep/Cap EVs were dose-matched to
424 EV-AAV2 by particle count as determined by nanoparticle tracking analysis. 100 µL of the diluted vector
425 was mixed with 900 µL of DMEM. As a negative control, 100 µL of PBS was mixed with 900 µL of DMEM.
426 Three groups of plates were made. Group 1 plates were treated with EV-AAV2, No Rep/Cap EVs, free
427 AAV2 or PBS for 4 h and analyzed by flow cytometry. Group 1 plates were used to measure fluorescence
428 associated with uptake of EVs at the time of cycloheximide or DMSO treatment. Plates in Group 2 and 3
429 were treated with EV-AAV2, No Rep/Cap EVs, free AAV2 or PBS for 4 h. After 4 h the media was removed
430 and replaced with fresh DMEM containing either 20 µg/mL cycloheximide dissolved in dimethyl sulfoxide
431 (DMSO) for Group 2 or DMSO at an equivalent volume for Group 3. 4 h post CHX or DMSO treatment,
432 Group 2 and Group 3 cells were analyzed by flow cytometry. In each group, the mean PE-Texas Red
433 fluorescence (AU) was determined across 3 treated wells and normalized to the mean fluorescence of PBS
434 treated cells within that group to facilitate comparisons across treatment groups.
435
436 ***Lentiviral vector production for Ultra-HEK analysis***
437 Lentivirus (LV) samples were produced in adherent Lenti-X cells seeded at a density of 3.2 x 10^5 cells/mL
438 in a volume of 0.5 mL DMEM in 24-well TC-treated plates 24 h prior to transfection. Cells were transfected
439 with 0.4 µg total DNA comprising 50% transfer vector, 29% gag/pol, 16% rev, and 5% VSV-G for the VSV-
440 G only composition and 46% transfer vector, 29% gag/pol, 16% rev, 5% VSV-G, and 4% Ultra-HEK for the
441 VSV-G and Ultra-HEK composition. The transfer vector used encodes constitutive expression of
442 mNeonGreen. Plasmids used for lentivirus production are Syenex's commercial plasmids: SNX-mNG-TV3,

443 SNX-Gagpol, SNX-Rev, SNX-VSV-G, and Ultra-HEK. Ultra-HEK is a plasmid designed to increase lentiviral
444 transduction of HEK293-derived cells. Plasmids and PEI MAX transfection reagent (Polysciences 24765)
445 were diluted in Opti-MEM and mixed in equal volumes at a 4:1 mass ratio of PEI to DNA and complexed
446 for 24 min prior to transfection. Medium was changed 12–16 h later. At least 28 h post media change, LV
447 was harvested from the conditioned medium and centrifuged at 1000 x g for 10 min at 4°C, then aliquoted
448 and stored at -80°C until use.
449
450 ***Analytical flow cytometry and analysis***
451 Most flow cytometry was performed on a BD LSR Fortessa Special Order Research Product using the
452 552 nm laser for mCherry or LumiScarlet (610/20 filter) and the 488 nm laser for eGFP or mNeonGreen
453 (530/30 filter). At least 10,000 live cells were collected per sample for analysis. Data were analyzed using
454 FlowJo v10 (FlowJo, LLC). Briefly, cells were identified using a forward scatter area (FSC-A) versus side
455 scatter area (SSC-A) plot and gated for single cells using an FSC-A versus forward scatter height (FSC-H)
456 plot (**Supplementary Information (Figures S1,S2,S3)**). Freestyle 293 cells were analyzed in the single
457 cells gate (**Figure S3**). HEK293FT (**Figure S1**) and Jurkat (**Figure S2**) live single cells were identified using
458 a DAPI-A versus SSC-A plot. Transduction was determined by the percentage of live single cells that were
459 brighter than approximately the 0.1% of the brightest cells in the untransduced (PBS treated) cell samples
460 (**Figure S1**). Mixed delivery was quantified by the mean of PE-Texas Red fluorescence of live single cells.
461 This mean fluorescence intensity was converted to MEPTRs by using UltraRainbow Calibration Particles
462 (Spherotech). Briefly, to determine the conversion from the arbitrary unit (au) of fluorescence recorded by
463 the flow cytometer to a standardized fluorescence unit (Molecules of Equivalent PE-TexasRed (MEPTR)),
464 UltraRainbow Calibration Particles were run as part of each flow cytometry experiment, except the AAV-
465 LumiScarlet experiment (**Figure 1**). This reagent contains nine subpopulations of beads, each of a specific
466 size and with a known intensity of various fluorophores, which are provided with calibration data for each
467 lot. The total bead population was identified by SSC-A vs. FSC-A gating, and subpopulations were identified
468 through two fluorescent channels (**Figure S4**). A calibration curve was generated for the experimentally
469 determined au vs. manufacturer supplied MEPTR, and a linear regression was performed with the
470 constraint that 0 au equals 0 MEPTR (**Figure S4B,** left). The slope from the regression was used as the

471 conversion factor. For experiments involving the quantification of mNeonGreen fluorescence intensity, the
472 mean FIT-C fluorescence of live single cells was converted to MEFLs by using UltraRainbow Calibration
473 Particles (Spherotech). Briefly, to determine the conversion from the arbitrary unit (au) of fluorescence
474 recorded by the flow cytometer to a standardized fluorescence unit (Molecules of Equivalent Fluorescein
475 (MEFLs)), UltraRainbow Calibration Particles were run as part of each flow cytometry experiment. A
476 calibration curve was generated for the experimentally determined au vs. manufacturer supplied MEFL,
477 and a linear regression was performed with the constraint that 0 au equals 0 MEFL (**Figure S4B,** right).
478 The slope from the regression was used as the conversion factor.
479
480 For experiments involving lentiviral transduction of HEK293T and HEK293FT by Ultra-HEK, similar methods
481 were used. Flow cytometry was performed on a Novocyte Penteon using the 488 nm laser for mNeonGreen
482 (525/45 filter) and the 637 nm laser for DRAQ7 (725/40 filter). Approximately 3,000 live cells were collected
483 per sample for analysis. Data were analyzed using FlowJo v10 (FlowJo, LLC). Briefly, cells were identified
484 using an FSC-A vs SSC-A plot and gated for singlets using an FSC-A vs FSC-H plot. Live cells were
485 identified using a DRAQ7 negative gate drawn on a non-DRAQ7-stained sample, and transduced cells
486 were identified by drawing an mNeonGreen positive gate on a non-transduced sample.
487
488 ***Transmission Electron Microscopy (TEM)***
489 For transmission electron microscopy (TEM), samples were diluted in PBS sterilized with 0.1 μm bottle top
490 filters (Corning 431475) to concentrations on the order of 10^8 particles per μL as determined by Nanoparticle
491 Tracking Analysis. Grids were plasma treated, and 3 μL of diluted sample were placed on the carbon side
492 of the grid for 30 s. The grids were then briefly washed on 3 droplets of distilled water and placed on a
493 droplet of stain solution (2% ammonium molybdate) for a few seconds. The staining solution was blotted
494 off and the grid was placed on a second droplet of staining solution for 30 s. Finally, the excess staining
495 solution was removed, and the grid was air-dried. Samples were observed with a JEOL 3200FS TEM at an
496 acceleration voltage of 300 kV. A K2 camera was used for recording images.
497
498 ***Western blots***

499 For western blots comparing protein in cell lysates and protein in vesicles, a fixed number of vesicles and
500 a fixed mass of cell lysate were loaded into each well: 4.5×10^8 EVs/lane and 2 µg protein/lane,
501 respectively. An established western blot protocol[48] was followed with the following modifications. In most
502 cases, the following reducing Laemmli composition was used to boil samples (60 mM Tris-HCl pH 6.8, 10%
503 glycerol, 2% sodium dodecylsulphate, 100 mM dithiothreitol (DTT) and 0.01% bromophenol blue); in some
504 cases, a nonreducing Laemmli composition (without DTT) was used, as previously reported[52]. After transfer,
505 membranes were blocked whilst rocking for 1 h at room temperature in 5% milk in Tris-buffered saline with
506 Tween (TBST) (pH: 7.6, 50 mm Tris, 150 mm NaCl, HCl to pH 7.6, 0.1% Tween 20). Primary antibody was
507 added in 5% milk in TBST, rocking, for 1 h at room temperature and then washed three times with TBST
508 for 5 min each. Secondary antibody in 5% milk in TBST was added at room temperature for 1 h or overnight
509 at 4°C. Membranes were then washed three times with TBST for 5 min each. The membrane was incubated
510 with Clarity Western ECL substrate (Bio-Rad, #1705061) and imaged on an Azure c280 running Azure
511 cSeries Acquisition software v1.9.5.0606. Specific antibodies, antibody dilution, heating temperature,
512 heating time and Laemmli composition for each antibody was used as previously reported[52].
513
514 ***Statistical analysis***
515 Statistical tests employed are described in relevant figure legends. Unless otherwise stated, three
516 independent technical replicates were analyzed per condition, and the mean fluorescence intensity of at
517 least 10,000 live single cells were analyzed per sample. Each figure represents a single experiment that
518 was repeated (biological replicate) at least twice. Unless otherwise indicated, error bars represent the
519 standard error of the mean. GraphPad Prism 10 was used to analyze the data. Multicomparison statistical
520 analysis was performed using a one-way ANOVA test, followed by Tukey's multiple comparison (i.e.,
521 honestly significant difference, HSD) test to evaluate specific comparisons. Significance threshold:
522 $*p < 0.05$, $**p < 0.01$, $***p < 0.001$, $****p < 0.0001$.
523
524 **RESULTS**
525
526 **Distinguishing pseudotransduction from transduction by EV-AAV is challenging**

527 We first sought to quantify the magnitude and dynamics of pseudotransduction for EV-AAV delivery
528 to HEK293FTs. It is commonly expected that the fluorescence conferred to recipient cells by EV-mediated
529 delivery of producer cell-derived protein and/or mRNA (i.e., pseudotransduction) will decrease over time
530 due to protein degradation and/or cell division, while fluorescence originating from transduction (gene
531 delivery and resulting transgene expression in recipient cells) will persist and increase to steady state.
532 However, the dynamics of such contributions are poorly explored and are likely to be system specific. To
533 characterize these phenomena in our model system, we utilized an AAV vector that constitutively expresses
534 a bright fluorescent protein, LumiScarlet, and we generated both EV-AAV (i.e., heterogeneous preps
535 expected to contain a mixture of EVs lacking any AAV particle and EVs associated with AAV particles) and
536 free AAV preparations (**Figure S5**). As a control for pseudotransduction, we included conditions lacking
537 Rep and Cap genes ("No Rep/Cap"). We sought to investigate both large and small EVs within our EV and
538 EV-AAV preparations, as both subsets have been shown to incorporate and deliver producer cell-derived
539 protein to recipient cells[28]. Therefore, a given EV-AAV or No Rep/Cap EV preparation contains both large
540 and small EVs. We also investigated several EV purification methods, including iodixanol gradient
541 purification[21,23,24] and size exclusion chromatography[25], reasoning that some fluorescent protein made by
542 producer cells may be excreted into the media along with free AAVs and EVs, and different EV purification
543 methods may remove these free proteins to different extents. Both purification methods yielded EVs with
544 expected protein markers (**Figures S6A,B**), appropriate size distributions (**Figure S6C**), and morphology
545 by TEM (**Figure S6D**). Purified vectors were dose-normalized (by genome count for EV-AAV and AAV with
546 No Rep/Cap EVs matched to EV-AAV by particle count) and delivered to HEK293FT cells (which actively
547 endocytose EVs). Fluorescence was monitored over 7 days by flow cytometry (**Figure 1, Figure S8**) and
548 microscopy (**Figure S7, Figure S9**). In general, fluorescence attributable to EV-AAV transduction was not
549 readily distinguished from fluorescence attributable to pseudotransduction (e.g., No Rep/Cap control). Free
550 AAV2 conferred distinguishable transgene expression in one experiment, which was distinguished by
551 quantifying the magnitude of fluorescence per cell (**Figure 1A, right**). Representative histograms of
552 LumiScarlet fluorescence from each sample also demonstrate that fluorescence attributable to EV-AAV
553 transduction was not readily distinguished from fluorescence attributable to protein delivery (**Figure 1B,**
554 **Figure S8B**). We noted that LumiScarlet fluorescence shifts leftward in these histograms over the time

555 course. Since this trend is observed across conditions, we hypothesize that cell division by these
556 proliferative HEK293FT cells dilutes both AAV genomes and LumiScarlet protein. Our analyses were
557 visually confirmed by microscopy (**Figure S7A-C, Figure S9A-C**), in which free AAV2 conferred the
558 expected whole cell fluorescence associated with de novo transgene expression, while EV conditions
559 exhibited puncta (which likely indicate the accumulation of multiple EVs in compartments such as
560 endosomes) that are readily apparent at 3 days post-treatment and remain detectable at 7 days post-
561 treatment. Transduction is apparent in images of EV-AAV and free AAV treated cells (but not No Rep/Cap
562 EV treated cells) by day 7, which is identifiable by diffuse and bright fluorescence throughout the cells. Our
563 analyses indicate that delivered protein is detectable (i.e., as puncta) in recipient cells for up to a week,
564 such that the time scale for delivered protein depletion and degradation is not readably separated from the
565 timescale of AAV episomal vector dilution (which may be particularly pronounced in these rapidly dividing
566 recipient cells). Overall, protein delivery by EV-AAVs may lead to significant pseudotransduction and is
567 challenging to distinguish from transduction regardless of EV purification method.
568

569 **A Cre recombinase-based dual reporter system enables discrimination between**
570 **pseudotransduction and transduction**

571 To address the challenge of pseudotransduction, we developed a novel Cre recombinase (Cre)-
572 based system to enable quantitative and unambiguous evaluation of gene and protein delivery by EV-AAVs.
573 We utilized a Cre-responsive AAV genome encoding a constitutive mCherry fluorescent protein that, upon
574 recombination, is excised to instead drive expression of a green fluorescent protein.[47] This dual-
575 fluorescence system enables visualization of producer cell-derived protein and/or mRNA delivery (mCherry)
576 and transduction (green) in Cre-expressing recipient cells. We initially investigated vector design in this
577 system using AAV and No Rep/Cap crude lysates; only the former should include transduction-competent
578 AAV particles (**Figure 2A**). Given a preceding Cre-responsive construct developed for a distinct purpose[47],
579 we generated several vectors to identify design choices that are useful for this application (**Figure 2B**). We
580 explored changing the transduction reporter from eGFP to mNeonGreen, hypothesizing that a brighter
581 fluorophore would help identify transduction. We also hypothesized that removing the nuclear localization
582 sequences (NLS) from the transduction reporter protein may increase accumulation in the recipient cell,

583 again facilitating detection. To evaluate these designs, we made Cre-expressing recipient HEK293FT cells
584 by lentiviral transduction.

585 We next evaluated the potential of each reporter system to ultimately detect pseudotransduction
586 and transduction. Each variant was packaged as either AAV2 crude lysate—which should include a mix of
587 free AAV2 and cell-derived fluorescent protein/mRNA—or a No Rep/Cap crude lysate control which should
588 include only cell-derived fluorescent protein/mRNA (and no transduction-competent AAV particles). Each
589 was delivered to Cre-expressing recipient cells or parental cell controls. Removal of the 3 x NLS generally
590 increased mCherry protein delivery, as expected, since the NLS sequesters some protein in the nucleus of
591 the producer cells (**Figure 2C, Figure S10A**). Greater mCherry fluorescence was observed in Cre-negative
592 than Cre-positive recipient cells, in samples treated with AAV2 crude lysate (i.e., which are expected to
593 include transduction competent AAV2 particles). A plausible explanation is that in recipient cells lacking Cre,
594 more mCherry gene expression occurs than when Cre is present, because in the former case a larger
595 fraction of the transgenes delivered by AAV transduction remain unrecombined. This suggests that the
596 decrease in mCherry expression in Cre+ cells (vs. Cre- cells) is consistent with recombination of the
597 transgene, switching from mCherry to green fluorescent protein production. The absence of this Cre-
598 expression-dependence in samples lacking AAV2 particles (i.e., No Rep/Cap conditions) supports this
599 interpretation. Most importantly, green fluorescent protein was detected only with AAV2 preps (i.e., crude
600 lysates containing transduction-competent vectors) delivered to Cre-expressing recipient cells (**Figure 2D,**
601 **Figure S10B**), validating this reporter system for unambiguously indicating transduction and de novo
602 transgene expression in recipient cells. Overall, the mNeonGreen vectors conferred higher percentages of
603 green positive live cells than did eGFP vectors, with the mNeonGreen vector without an NLS performing
604 the best. On balance, going forward we selected the vector with mNeonGreen and the 3 x NLS, since it
605 conferred more green-positivity in Cre-expressing recipient cells compared to eGFP vectors (i.e., greater
606 signal), and it conferred less mCherry fluorescence compared to vectors without an NLS (i.e., lower
607 background).

608 We next interrogated several aspects of our reporter system. First, we probed whether any leaky
609 mNeonGreen expression occurred in producer cells, as spontaneous recombination has been reported in
610 other Cre responsive plasmids[53,54]. If spontaneous recombination occurs, mNeonGreen protein may be

611 expressed and loaded into EVs, as could mNeonGreen mRNA, resulting in mNeonGreen detection in
612 recipient cells. To test this possibility we examined EV-AAV producer cells 3 d after transfection (**Figure**
613 **S11**). We observed very low (but detectable) mNeonGreen expression in ~11% of cells transfected with our
614 AAV plasmids, and a similar frequency was observed in the Stoplight only (No Rep/Cap) condition, such
615 that this leakiness was not impacted by AAV genome replication and packaging. In contrast, controls
616 including Cre recombinase in EV-AAV producer cells yielded approximately 60% mNeonGreen positive
617 cells and much higher magnitudes of mNeonGreen expression. Thus, despite some evidence of
618 spontaneous recombination of our stoplight plasmid in EV producer cells, not much mNeonGreen protein
619 is produced during the timescale of our transfections, which helps to explain why no mNeonGreen was
620 detected in recipient cells except when both AAV and Cre were present (**Figure 2D, Figure S10B**). To
621 further test this interpretation, we repeated our initial delivery experiment based upon crude lysate (**Figure**
622 **2D, Figure S10B**) using SEC purified EVs and purified free AAV (**Figure S12**) and again found that
623 mNeonGreen transfer (protein and/or mRNA) by EV-AAV preps (and by No Rep/Cap control EVs) is
624 minimal.

625 Finally, we explored the source of the mCherry signal observed in recipient cells. mCherry
626 expression in recipient cells could result from delivery of producer cell derived protein by EVs, producer cell
627 derived mRNA and subsequent translation in recipient cells, or de novo mCherry produced by the
628 unrecombined transgene delivered by EV-AAVs. To investigate the possibility that producer cell derived
629 mRNA contributes to mCherry signal, we utilized a protocol previously used to investigate mRNA delivery
630 by engineered EVs[44] (**Figure S13A**). Cells were treated with EV-AAVs, No Rep/Cap EVs, or Free AAV and
631 fluorescence was assessed after 4 hours. As second group of cells were similarly treated with vectors for 4
632 h, but then 20 μg/mL of the translation inhibitor cycloheximide (CHX) was added and fluorescence was
633 assessed after another 4 h had elapsed. Overall, there was minimal decrease in fluorescence in cells
634 treated with cycloheximide and either EV-AAVs or No Rep/Cap EVs compared to DMSO-treated controls
635 (**Figure S13B,C**). These results suggest that at least at early timepoints, most mCherry fluorescence
636 observed in recipient cells treated with EVs or EV-AAVs originates from producer cell-derived mCherry
637 protein. Nonetheless, to encompass the possibility that mCherry signal in recipient cells could derive from
638 protein delivery, mRNA delivery, and/or AAV delivery (for conditions contain transduction-competent AAV

639 particles), we henceforth conservatively describe these phenomena collectively as “mixed delivery”. We
640 carried this validated reporter system forward to probe EV-AAV bioengineering questions.
641
642 **EV-AAV2 surface functionalization substantially increases mixed delivery but not transduction of**
643 **HEK293FTs**
644 We next investigated how EV functionalization strategies that have been reported to increase
645 delivery of lentiviruses or EVs impact mixed delivery and transduction by EV-AAV. VSV-G is often used in
646 pseudotyping lentiviruses[55,56] and EVs[57,58], and it increases the protein delivered by EVs.[58] VSV-G binds to
647 the LDL receptor (LDL-R) on the surface of recipient cells[30], increasing particle uptake as a result. Within
648 the low pH of the endosome, VSV-G undergoes conformational changes that enable it to promote fusion
649 between the viral (or EV) membrane and the endosomal membrane to release the vector’s luminal contents
650 into the cytosol of the recipient cell.[59] To separate the impacts of enhancing uptake and mediating fusion,
651 we also utilized Ultra-HEK, a commercial product (Syenex) that increases lentiviral transduction of HEK293-
652 based cells when combined with a fusogen such as VSV-G. Ultra-HEK is described as interacting with
653 proteins on the surface of recipient HEK293 cells to cause increased uptake of the particle (but not fusion).
654 In our hands, packing lentiviral vectors with Ultra-HEK led to increased transduction (i.e., functional titer)
655 for delivery to both HEK293T cells and HEK293FT cells (**Figure 3A–C**).
656 Using our reporter system and this menu of surface functionalization strategies (**Figure 3D, Figure**
657 **S14A**), we revisited the question of how driving EV-AAV uptake (and/or fusion) impacts transduction
658 efficiency. All functionalization strategies increased mixed delivery, as measured by either the magnitude
659 mCherry fluorescence (**Figure 3E,** left and **Figure S14B,** left) or frequency of mCherry positive cells (**Figure**
660 **3E,** right and **Figure S14B,** right), likely due to increased particle uptake by recipient cells. Ultra-HEK
661 combined with VSV-G functionalization increased mixed delivery to the greatest extent compared to non-
662 targeted EV-AAV2. Since doses of EV-AAVs were normalized by genome copy, it is possible that equivalent
663 genome doses comprise distinct numbers of EVs. To exclude the possibility that this could explain the mixed
664 delivery trend, we plotted mixed delivery by EV dose (in particle count), and we found that this does not
665 well explain our observations (**Figure S15**). Thus, differences in mixed delivery are best explained by the
666 biological effects of our functionalization strategies. Interestingly, surface functionalization did not increase

667 transduction to the same degree as it did protein delivery, with transduction measured by either magnitude
668 of mNeonGreen fluorescence (**Figure 3F,** left and **Figure S14C,** left) or frequency of mNeonGreen positive
669 cells (**Figure 3F,** right and **Figure S14C,** right). Only the dual functionalization strategy modestly increased
670 the amount of transduction of HEKs over non-targeted vectors, and there was no evidence that fusion
671 mediated by VSV-G enhanced or blocked EV-AAV transduction. Given this comparison, going forward, we
672 chose metrics that are most aligned with the phenomenon being evaluated. We reasoned that degree of
673 fluorescence conferred by mixed delivery is a continuous variable, and therefore mean fluorescence
674 captures variation in that signal. Conversely, transduction is digital (transduced vs. not transduced), even if
675 transduced cells vary in their degree of mNeonGreen expression; therefore, frequency of mNeonGreen+
676 cells is the metric most aligned with that measurement. Finally, we noted that the vast majority of cells that
677 were truly transduced (mNeonGreen+) also were mCherry+ (i.e., mNeonGreen+/mCherry- cells were
678 vanishingly rare), and this pattern was true across functionalization strategies (**Figure S16**). These findings
679 led us to investigate whether these trends extend to other serotypes and recipient cells.
680
681 **EV-AAV6 surface functionalization increases mixed delivery and transduction of Jurkat T cells**
682 We next explored EV-AAV delivery to a cell type with low spontaneous EV uptake. We chose to
683 use human Jurkat T cells, which are somewhat recalcitrant to EV-based delivery due (at least in part) to
684 low endocytosis.[28] We transduced Jurkats with the Cre recombinase gene to make a recipient line
685 compatible with our dual reporter system. We used AAV6 as it infects both primary T cells[60] and Jurkats[61].
686 We focused on VSV-G functionalization which mediates lentiviral transduction of T cells via LDL-R binding
687 and uptake (**Figure 4A, Figure S17A**).[62] Similar to HEK293FT delivery (**Figure 3, Figure S14**), VSV-G
688 functionalization increased mixed delivery to Jurkats compared to non-targeted EV-AAV6 (**Figure 4B,**
689 **Figure S17B**). Surprisingly, and unlike in HEK293FT recipient cells, VSV-G functionalization also increased
690 transduction of Jurkats (**Figure 4C, Figure S17C**).
691 This led us to investigate what mechanism conferred by VSV-G (uptake vs. fusion) contributed to
692 increased transduction. We employed two VSV-G mutants to dissect these mechanisms (**Figure 4D, Figure**
693 **S17D**). P127D retains the ability to bind to LDL-R but is deficient in membrane fusion.[49,63,64] Conversely,
694 mutations K47Q-R354A block LDL-R binding but still enable VSV-G to confer membrane fusion.[65-67] Wild-

695 type (WT) and P127D VSV-G functionalization resulted in more mixed delivery than did K47Q-R354A or
696 non-targeted vectors (**Figure 4E, Figure S17E**). Interestingly, the K47Q-R354A VSV-G conferred less
697 transduction than did the WT or P127D VSV-G vectors, indicating that binding to LDL-R on recipient cells
698 is the dominant mechanism by which VSV-G increases transduction of Jurkat T cells (**Figure 4F, Figure**
699 **S17F**). Notably, P127D VSV-G, which is fusion incompetent, conferred more transduction than did VSV-G
700 WT vectors. Altogether, these results may indicate that for EV-AAV6 delivery to Jurkats, increased LDL-R
701 binding increases particle uptake and transduction, while membrane fusion limits transduction.

702 We next investigated whether the trend of double positive cells we observed in our HEK delivery
703 experiments (**Figure S16)** held for Jurkat delivery experiments (**Figure S18**). We utilized the mutant VSV-
704 G data sets to explore this question. Surprisingly, and contrasting with our HEK delivery experiments, most
705 truly transduced Jurkat cells (mNeonGreen+) were mCherry- (**Figure S18B,C).** This difference may be
706 explained by the relatively low uptake (endocytosis) rate of EVs by Jurkats compared to HEKs, as
707 evidenced by the low frequency of mixed delivery signal overall compared to HEKs. Additionally, the vectors
708 with functionalization that improves uptake (VSV-Gwt and P127D) demonstrated more cells that were
709 double positive than the uptake incompetent vectors (VSV-G K47Q 354A and non-targeted). Overall, this
710 analysis illustrates how the stoplight vector enables one to probe multiple aspects of delivery and compare
711 across cell types.

712

713 **Recipient cell type but not capsid serotype drives the impact of functionalization on EV-AAV delivery**

714 To reconcile the distinct patterns observed in our HEK293FT and Jurkat delivery experiments, we
715 investigated whether differences are driven primarily by recipient cell type or AAV serotype. We chose to
716 investigate transducing HEK293FT cells with AAV6 since AAV6 is much less efficient at infecting
717 HEK293FTs compared to AAV2.[61] This difference may be due to differences in receptor density on the
718 surface of HEKs. AAV2 primarily uses heparan sulfate proteoglycan to mediate binding and uptake by
719 recipient cells.[68] In contrast, AAV6 primarily uses sialic acid as its receptor[68], which may be less abundant
720 or accessible on HEK293 cells compared to heparan sulfate proteoglycan. Therefore, we hypothesized that
721 increasing uptake of EV-AAV6 (e.g., via VSV-G functionalization) would increase transduction compared to
722 both non-targeted EV-AAV6 or free AAV6 (**Figure 5A, Figure S19A**). VSV-G functionalization increased

723 mixed delivery compared to non-targeted EV-AAV6, as expected (**Figure 5B, Figure S19B**). However,
724 VSV-G mediated uptake (and fusion) did not increase transduction by EV-AAV6 (**Figure 5C, Figure S19C**),
725 as was seen for EV-AAV2 (**Figure 3F, Figure S14D**). Thus, increasing uptake and membrane fusion in a
726 cell type that is permissible to EV delivery, such as HEK293FTs, did not increase transduction, regardless
727 of AAV capsid choice. With the set of conditions evaluated, EV surface functionalization strategies conferred
728 cell type-dependent but not capsid-dependent effects on transduction by EV-AAVs.
729

730 **DISCUSSION**

731 Engineered EVs are promising delivery vehicles for AAV vectors, enabling tissue-specific targeting and
732 neutralizing antibody evasion. However, analyzing and bioengineering such vectors is made challenging by
733 the difficulty associated with distinguishing pseudotransduction from transduction. To address this need, in
734 this study we developed and validated a new assay that unambiguously distinguishes transduction from
735 mixed delivery (including pseudotransduction), while enabling quantification of both phenomena. This
736 assay helped to generate new insights that inform both interpretation of past studies and identify
737 opportunities for future investigation.

738 Our observations provide new insights that help to interpret apparent contradictions in the EV-AAV
739 literature. A prior report indicated that pseudotyping EV-AAV2 with VSV-G decreased the transduction of
740 HEK293 cells compared to non-targeted EV-AAV2.[69] Notably, this analysis employed a luminescence-
741 based plate reader assay, and it may have been confounded by pseudotransduction artifacts. Our results
742 suggest that VSV-G neither improves, nor hinders EV-AAV2 transduction of HEKs (**Figure 3**, **Figure S14**).
743 Interestingly, our results suggest that VSV-G does improve transduction of EV-AAV6 in Jurkats by
744 increasing particle uptake (**Figure 4, Figure S17**). Overall, our work suggests that the effects of surface
745 functionalization on EV-AAV transduction is cell type dependent.

746 Some previous studies report that EV-AAVs are more potent than AAV vectors for *in vivo* delivery (on
747 a per genome basis)[14-16,22], but other work focused on delivery to neuronal and primary astrocyte cell
748 cultures seemingly contradicts this finding[70]. It is possible that improved *in vivo* efficacy of EV-AAV particles
749 is primarily attributable not to the enhanced interaction between the AAV and the target cells, but rather to
750 shielding of AAVs from neutralizing antibodies and/or biodistribution effects such as increased circulation

751 time or improved delivery through tissue barriers. Our observations add another layer of possible
752 explanation, given our finding that target cell type and capsid choice may impact the efficacy of EV-AAV
753 compared to free AAV. Free AAV2 was significantly more potent for transduction in HEK293FTs compared
754 to non-targeted EV-AAV2 (**Figure 3, Figure S14**). However, non-targeted EV-AAV6 outperformed (**Figure**
755 **5)** or was equivalent to (**Figure S19**) free AAV6 in transduction in HEK293FTs. This suggests that capsid
756 choice may impact the relative transduction efficacy of EV-AAV and free AAV. EV-AAV6 was not statistically
757 significantly different from free AAV6 in transduction of Jurkat T cells (**Figure 4, Figure S17**), further
758 suggesting that the capsid choice may impact efficacy comparisons between EV-AAV and free AAV. Overall,
759 our findings indicate that the impact of EV-encapsulation of AAV confers case-specific effects that should
760 be evaluated for each application, and which may drive application-specific bioengineering.

761 This study focused on identifying high level determinants of functional delivery, yet it also identified
762 opportunities for further subsequent mechanistic investigations. Pseudotransduction was more evident in
763 HEK293FT recipient cells, which actively endocytose EVs, compared to Jurkat recipient cells, which exhibit
764 less endocytosis. Increasing EV uptake via surface functionalization also increased pseudotransduction in
765 both cell types. Increasing the uptake of EV-AAV to HEK293FT recipient cells, both with or without
766 promoting membrane fusion, increased mixed delivery, but this did not substantially increase transduction
767 for either EV-AAV2 or EV-AAV6. However, VSV-G functionalization of EV-AAV6 increased both mixed
768 delivery and transduction of Jurkat T cells, and this effect was driven primarily by increased uptake rather
769 than fusion; indeed, blocking VSV-G-mediated fusion via the P127D mutant enhanced transduction. The
770 basis for these differences is not known, but a possible explanation is that AAV requires processing in the
771 endosome—including capsid cleavage by endosomal cathepsins[31] and acidification-mediated
772 autoproteolytic processing[32]—to expose a phospholipase domain promoting virion escape and subsequent
773 nuclear trafficking[33,34]. In prior work, microinjection of AAV2 particles directly into the cytosol resulted in no
774 nuclear trafficking and subsequent transduction[71], suggesting that endosomal processing of the AAV capsid
775 is required for successful transduction. This requirement is well-characterized for free AAV2 and may extend
776 to other serotypes.

777 Combining these observations enables one to propose potential explanatory mechanisms as to how
778 different EV surface functionalizations impact transduction. First, it is possible that VSV-G confers improved

779 EV-AAV6 uptake by Jurkats, overcoming one barrier to delivery, but VSVG-mediated membrane fusion
780 circumvents the endosomal processing of the AAV6 capsid that is required to complete transduction. Thus,
781 the VSV-G P127D mutant balances these effects to benefit delivery to T cells. It would be informative to
782 probe how each step in capsid processing is impacted by encapsulation in EVs, and how such processing
783 steps may differentially impact AAV particles on the EV surface versus the EV interior. In addition, directly
784 tracking internalization of both receptors and particles could help to test the mechanisms offered as
785 speculative explanations here. A second, non-exclusive hypothesis for explaining improved transduction of
786 Jurkats by EVs functionalized with the VSV-G P127D mutant is that this vector confers enhanced EV uptake
787 compared to WT VSV-G, as evidenced by increased mixed delivery signal (**Fig 4E** and **Fig S17E**). No such
788 mechanism is yet known, but it is possible that the P127D mutant is expressed at higher levels on EVs, is
789 internalized more rapidly, or drives different trafficking after uptake. A final non-exclusive hypothesis
790 involves innate immune activation. It is possible that WT VSV-G induces membrane fusion to prompt or
791 enhance innate immune responses such as interferon production, which dampen transgene expression in
792 cells transduced by AAV[72]. Elucidating such contributors to successful delivery (e.g., transgene expression
793 magnitude as a function of vgDNA dose) could build upon these observations to improve EV-AAV
794 engineering.

795 It will be interesting to extend these studies to the many AAV capsid variants that exist, including natural
796 serotypes as well as novel forms developed through directed evolution and protein engineering[73], and to a
797 variety of recipient cell types including those which endocytose EVs more readily than do HEK293FTs[74].
798 This work could also enable new AAV bioengineering campaigns specific to enhancing EV-AAV delivery,
799 such as exploring mutations that destabilize the capsid structure to enhance transduction after EV fusion
800 and delivery of the AAV core to the cytosol, bypassing endosomal processing.

801 There exist a number of opportunities for extending the approaches and methods reported here to study
802 aspects of EV biology beyond those probed in this investigation. First and foremost, there exist many
803 different methods for producing and purifying EV-AAV particles, and choice of method is likely to affect the
804 biology, composition, and function of the resulting particles. Our EV harvesting method utilized differential
805 centrifugation to remove cells (300 g x 10 min) and cell debris/apoptotic bodies (2000 g x 20 min), followed
806 by tangential flow filtration to concentrate the supernatant. This choice intentionally includes a mixture of

807 EVs in our samples (our EV characterizations by nanoparticle tracking analysis, western blots, and TEM
808 (**Figure S6**) demonstrate the purity of our preparations). Although the MISEV2023 guidelines for EV
809 research indicate that EV preparations pelleted at different centrifugation speeds (i.e., “small” and “large”
810 EVs) contain EVs with overlapping size profiles[75], and EVs are heterogenous in size and associated
811 contents regardless of purification method[76,77], it would nonetheless be interesting to employ our stoplight
812 assay to evaluate whether EV-AAV fractions that pellet at different speeds, or which are isolated with
813 different purification methods, confer different levels of pseudotransduction and transduction. Our EV-AAV
814 preparations certainly contain both EVs that lack AAV and EVs that are associated with AAV.[17] If methods
815 to isolate EVs containing AAVs were available, and to segregate by EV-surface versus EV-interior loading
816 of AAV, it would be particularly interesting to analyze how these subsets contribute to transduction and
817 pseudotransduction. It would also be interesting to study how EV-AAV delivery phenomena change over a
818 broader dose range. In our studies, the MOI as defined by transducing units per cell is rather low, such that
819 we were far from the saturating regime of EV-AAV transduction. Accessing that higher MOI regime could
820 be made feasible through improvements such as recently reported methods for enhancing AAV loading into
821 EVs.[38] Each of these represents an opportunity for leveraging our stoplight method to improve
822 understanding of EV-AAV mediated delivery.

823 Our analysis provides an opportunity to speculate as to how pseudotransduction may, or may not,
824 influence other investigations of EV-AAV. Many *in vitro* and *in vivo* studies of EV-AAVs have been
825 performed, delivering transgenes including luciferases, fluorescent proteins, and therapeutic genes. A
826 potential factor in detecting pseudotransduction by EV-AAVs is the half-life of the transgenic protein in
827 recipient cells. EV-AAV preparations encoding firefly luciferase but lacking the capsid protein (equivalent to
828 our No Rep/Cap EV samples) have previously been compared to EV-AAV-FLuc (with the capsid protein) in
829 transduction of HELA cells[23]. Capsid-less EV-AAV-FLuc conferred low FLuc activity (2-fold above
830 background levels) whereas EV-AAV conferred 9-fold higher FLuc activity compared with the capsid-less
831 EV-AAV genomes. Since this suggests a lower degree of pseudotransduction, it is possible that compared
832 to FLuc, fluorescent proteins may resist degradation in the endosomal lysosomal compartment (which is
833 distinct from half-life measured in the cytosol). Thus, choice of reporter transgene may mitigate, but not
834 necessarily avoid, pseudotransduction artifacts, at least on the relatively short time scales of *in vitro* delivery

835 experiments using rapidly dividing cells (where dilution of AAV genomes constrains the time one can wait
836 post-delivery to analyze transduction). Our stoplight system may be particularly enabling for such
837 experiments.

838 An exciting prospect is extending this assay for *in vivo* EV-AAV delivery analyses. The stoplight vector
839 inspiring our approach was originally employed to detect Cre expression *in vivo*[47]. Given that transgenic
840 animals can be engineered to express Cre in a tissue-restricted or general fashion[78], our assay could be
841 employed to unambiguously identify EV-AAV transduction *in vivo*. Such a capability could be particularly
842 useful for directly comparing AAV and EV-AAV-mediated delivery, and for enabling comparative evaluation
843 of bioengineering approaches, *in vivo* multiplexed screening, and other efforts for which pseudotransduction
844 is misleading or reduces signal-to-noise to preclude feasibility. Because most *in vivo* studies of EV-AAV
845 wait days to weeks after EV-AAV treatment to analyze transduction, pseudotransduction artifacts may have
846 diminished by the time of analysis, but that is unproven and merits examination, especially for slow-dividing
847 recipient cells. This stoplight tool could probe whether pseudotransduction is indeed negligible, and even if
848 it is, this tool could enable faster, unambiguous evaluation of *in vivo* transduction. We expect that the
849 methods and findings presented here can help advance the understanding and use of EV-AAV vectors for
850 diverse gene delivery applications.

851

852 **AUTHOR CONTRIBUTIONS**

853 J.D.B., D.M.S., N.P.K., D.T.E., and J.N.L. conceived the initial project. J.D.B. performed the experiments.
854 D.M.S. and H.I.E. performed the Ultra-HEK lentiviral vector experiment. J.D.B. and J.N.L. planned and
855 analyzed experiments. J.D.B and J.N.L. wrote the manuscript. J.N.L. supervised the work.

856

857 **ACKNOWLEDGEMENTS**

858 J.D.B. was supported by the National Institutes of Health Training Grant (T32GM008449) through
859 Northwestern University's Biotechnology Training Program. J.D.B was supported by the National Science
860 Foundation Graduate Research Fellowship under grant number (DGE-1842165). This project was partially
861 supported by an award from the McCormick Catalyst Fund (J.N.L.) and by a Cornew Innovation Award from
862 the Chemistry of Life Processes Institute at Northwestern University (J.N.L.). Flow Cytometry was

performed in the Northwestern University Flow Cytometry Core Facility supported by Cancer Center Support Grant (NCI CA060553) and in the Single Cell Genomics Facility at Northwestern University (RRID:SCR_026652), graciously supported by the Department of Neurobiology, the Department of Molecular Biosciences, and the NU Office for Research. This work made use of the BioCryo Core (RRID:SCR_021288) of Northwestern University's NUANCE Center, which has received support from the SHyNE Resource (NSF ECCS-2025633), the IIN, and Northwestern's MRSEC program (NSF DMR-2308691). Biological analysis] was performed in the Analytical bioNanoTechnology Equipment Core Facility of the Center for Regenerative Nanomedicine at Northwestern University. ANTEC receives partial support from the Soft and Hybrid Nanotechnology Experimental (SHyNE) Resource (NSF ECCS-2025633) and Feinberg School of Medicine, Northwestern University. This work was supported by the Northwestern University Sanger Sequencing Facility. Any opinion, findings and conclusions or recommendations expressed in this material are those of the authors and do not necessarily reflect the views of the National Science Foundation. The authors kindly thank the Leonard lab members for useful discussions throughout the planning, experimental, analysis and writing phases of this project. The authors would like to thank Dmitriy Bobrovnikov and Roxi Mitrut for discussions of Cre-responsive AAV vectors.

DECLARATION OF INTERESTS STATEMENT

J.N.L., D.M.S. and H.I.E. have financial interests in Syenex Inc., which could potentially benefit from the outcomes of this research.

883 **REFERENCES**

884 1 Wang, J.-H., Gessler, D. J., Zhan, W., Gallagher, T. L. & Gao, G. Adeno-associated virus as a
885 delivery vector for gene therapy of human diseases. *Signal Transduction and Targeted Therapy* **9**,
886 78 (2024). https://doi.org:10.1038/s41392-024-01780-w

887 2 Earley, J., Piletska, E., Ronzitti, G. & Piletsky, S. Evading and overcoming AAV neutralization in
888 gene therapy. *Trends in Biotechnology* **41**, 836-845 (2023).
889 https://doi.org:https://doi.org/10.1016/j.tibtech.2022.11.006

890 3 Srivastava, A. In vivo tissue-tropism of adeno-associated viral vectors. *Current Opinion in Virology*
891 **21**, 75-80 (2016). https://doi.org:https://doi.org/10.1016/j.coviro.2016.08.003

892 4 Duan, D. Lethal immunotoxicity in high-dose systemic AAV therapy. *Molecular Therapy* **31**, 3123-
893 3126 (2023). https://doi.org:https://doi.org/10.1016/j.ymthe.2023.10.015

894 5 Hordeaux, J. *et al.* High-dose systemic adeno-associated virus vector administration causes liver
895 and sinusoidal endothelial cell injury. *Molecular Therapy* **32**, 952-968 (2024).
896 https://doi.org:https://doi.org/10.1016/j.ymthe.2024.02.002

897 6 Raposo, G. & Stoorvogel, W. Extracellular vesicles: exosomes, microvesicles, and friends. *J Cell*
898 *Biol* **200**, 373-383 (2013). https://doi.org:10.1083/jcb.201211138

899 7 Cocucci, E., Racchetti, G. & Meldolesi, J. Shedding microvesicles: artefacts no more. *Trends Cell*
900 *Biol* **19**, 43-51 (2009). https://doi.org:10.1016/j.tcb.2008.11.003

901 8 Valadi, H. *et al.* Exosome-mediated transfer of mRNAs and microRNAs is a novel mechanism of
902 genetic exchange between cells. *Nat Cell Biol* **9**, 654-659 (2007). https://doi.org:10.1038/ncb1596

903 9 Mizrak, A. *et al.* Genetically engineered microvesicles carrying suicide mRNA/protein inhibit
904 schwannoma tumor growth. *Mol Ther* **21**, 101-108 (2013). https://doi.org:10.1038/mt.2012.161

905 10 Andaloussi, E. L., Mager, I., Breakefield, X. O. & Wood, M. J. Extracellular vesicles: biology and
906 emerging therapeutic opportunities. *Nature reviews. Drug discovery* **12**, 347-357 (2013).
907 https://doi.org:10.1038/nrd3978

908 11 Gyorgy, B., Hung, M. E., Breakefield, X. O. & Leonard, J. N. Therapeutic applications of
909 extracellular vesicles: clinical promise and open questions. *Annual review of pharmacology and*
910 *toxicology* **55**, 439-464 (2015). https://doi.org:10.1146/annurev-pharmtox-010814-124630

911 12 Marcus, M. E. & Leonard, J. N. FedExosomes: Engineering Therapeutic Biological Nanoparticles
912 that Truly Deliver. *Pharmaceuticals-Base* **6**, 659-680 (2013). https://doi.org:10.3390/ph6050659
913 13 Maguire, C. A. *et al.* Microvesicle-associated AAV vector as a novel gene delivery system. *Mol Ther*
914 **20**, 960-971 (2012). https://doi.org:10.1038/mt.2011.303
915 14 Hudry, E. *et al.* Exosome-associated AAV vector as a robust and convenient neuroscience tool.
916 *Gene Therapy* **23**, 380-392 (2016). https://doi.org:10.1038/gt.2016.11
917 15 György, B. *et al.* Rescue of Hearing by Gene Delivery to Inner-Ear Hair Cells Using Exosome-
918 Associated AAV. *Molecular Therapy* **25**, 379-391 (2017).
919 https://doi.org:https://doi.org/10.1016/j.ymthe.2016.12.010
920 16 Wassmer, S. J., Carvalho, L. S., György, B., Vandenberghe, L. H. & Maguire, C. A. Exosome-
921 associated AAV2 vector mediates robust gene delivery into the murine retina upon intravitreal
922 injection. *Scientific Reports* **7**, 45329 (2017). https://doi.org:10.1038/srep45329
923 17 Meliani, A. *et al.* Enhanced liver gene transfer and evasion of preexisting humoral immunity with
924 exosome-enveloped AAV vectors. *Blood Adv* **1**, 2019-2031 (2017).
925 https://doi.org:10.1182/bloodadvances.2017010181
926 18 Breuer, C. B. *et al.* In vivo engineering of lymphocytes after systemic exosome-associated AAV
927 delivery. *Scientific Reports* **10**, 4544 (2020). https://doi.org:10.1038/s41598-020-61518-w
928 19 Liu, B. *et al.* AAV-Containing Exosomes as a Novel Vector for Improved Gene Delivery to Lung
929 Cancer Cells. *Frontiers in Cell and Developmental Biology* **Volume 9 - 2021** (2021).
930 https://doi.org:10.3389/fcell.2021.707607
931 20 Kwak, G. *et al.* Extracellular vesicles enhance pulmonary transduction of stably associated adeno-
932 associated virus following intratracheal administration. *Journal of Extracellular Vesicles* **12**, 12324
933 (2023). https://doi.org:https://doi.org/10.1002/jev2.12324
934 21 Li, X. *et al.* Extracellular Vesicle–Encapsulated Adeno-Associated Viruses for Therapeutic Gene
935 Delivery to the Heart. *Circulation* **148**, 405-425 (2023).
936 https://doi.org:10.1161/CIRCULATIONAHA.122.063759

937 22 György, B., Fitzpatrick, Z., Crommentuijn, M. H. W., Mu, D. & Maguire, C. A. Naturally enveloped
938 AAV vectors for shielding neutralizing antibodies and robust gene delivery in vivo. *Biomaterials* **35**,
939 7598-7609 (2014). https://doi.org:https://doi.org/10.1016/j.biomaterials.2014.05.032
940 23 Cheng, M. *et al.* Probing aspects of extracellular vesicle associated AAV allows increased vector
941 yield and insight into its transduction and immune-evasive properties. *Mol Ther Methods Clin Dev*
942 **33**, 101407 (2025). https://doi.org:10.1016/j.omtm.2025.101407
943 24 Espinoza, P. *et al.* Metabolic engineering improves transduction efficiency and downstream vector
944 isolation by altering the lipid composition of extracellular vesicle-enclosed AAV. *Metabolic*
945 *Engineering* **88**, 40-49 (2025). https://doi.org:https://doi.org/10.1016/j.ymben.2024.12.003
946 25 Cheng, M. *et al.* Neutralizing Antibody Evasion and Transduction with Purified Extracellular Vesicle-
947 Enveloped Adeno-Associated Virus Vectors. *Hum Gene Ther* **32**, 1457-1470 (2021).
948 https://doi.org:10.1089/hum.2021.122
949 26 Alvarez-Erviti, L. *et al.* Delivery of siRNA to the mouse brain by systemic injection of targeted
950 exosomes. *Nat Biotechnol* **29**, 341-345 (2011). https://doi.org:10.1038/nbt.1807
951 27 Murphy, D. E. *et al.* Extracellular vesicle-based therapeutics: natural versus engineered targeting
952 and trafficking. *Experimental & molecular medicine* **51**, 1-12 (2019).
953 28 Stranford, D. M. *et al.* Genetically encoding multiple functionalities into extracellular vesicles for the
954 targeted delivery of biologics to T cells. *Nat Biomed Eng* **8**, 397-414 (2024).
955 https://doi.org:10.1038/s41551-023-01142-x
956 29 Wiklander, O. P. B. *et al.* Antibody-displaying extracellular vesicles for targeted cancer therapy.
957 *Nature Biomedical Engineering* **8**, 1453-1468 (2024). https://doi.org:10.1038/s41551-024-01214-6
958 30 Finkelshtein, D., Werman, A., Novick, D., Barak, S. & Rubinstein, M. LDL receptor and its family
959 members serve as the cellular receptors for vesicular stomatitis virus. *Proceedings of the National*
960 *Academy of Sciences* **110**, 7306-7311 (2013). https://doi.org:doi:10.1073/pnas.1214441110
961 31 Akache, B. *et al.* A two-hybrid screen identifies cathepsins B and L as uncoating factors for adeno-
962 associated virus 2 and 8. *Mol Ther* **15**, 330-339 (2007). https://doi.org:10.1038/sj.mt.6300053
963 32 Salganik, M. *et al.* Evidence for pH-dependent protease activity in the adeno-associated virus
964 capsid. *J Virol* **86**, 11877-11885 (2012). https://doi.org:10.1128/jvi.01717-12

965 33 Girod, A. *et al.* The VP1 capsid protein of adeno-associated virus type 2 is carrying a phospholipase
966 A2 domain required for virus infectivity. *J Gen Virol* **83**, 973-978 (2002).
967 https://doi.org:10.1099/0022-1317-83-5-973
968 34 Stahnke, S. *et al.* Intrinsic phospholipase A2 activity of adeno-associated virus is involved in
969 endosomal escape of incoming particles. *Virology* **409**, 77-83 (2011).
970 https://doi.org:10.1016/j.virol.2010.09.025
971 35 Guo, Y. *et al.* Early events in rabies virus infection-Attachment, entry, and intracellular trafficking.
972 *Virus Res* **263**, 217-225 (2019). https://doi.org:10.1016/j.virusres.2019.02.006
973 36 Gaudin, Y. Rabies Virus-Induced Membrane Fusion Pathway. *Journal of Cell Biology* **150**, 601-612
974 (2000). https://doi.org:10.1083/jcb.150.3.601
975 37 Albertini, A. A., Baquero, E., Ferlin, A. & Gaudin, Y. Molecular and cellular aspects of rhabdovirus
976 entry. *Viruses* **4**, 117-139 (2012). https://doi.org:10.3390/v4010117
977 38 Vorobieva, I. *et al.* Engineered AAV Capsids with Enhanced Extracellular Vesicle Loading via
978 Rational Design and Directed Evolution. *bioRxiv*, 2025.2012.2012.693981 (2025).
979 https://doi.org:10.64898/2025.12.12.693981
980 39 Haas, D. L., Case, S. S., Crooks, G. M. & Kohn, D. B. Critical Factors Influencing Stable
981 Transduction of Human CD34+ Cells with HIV-1-Derived Lentiviral Vectors. *Molecular Therapy* **2**,
982 71-80 (2000). https://doi.org:https://doi.org/10.1006/mthe.2000.0094
983 40 Galla, M., Will, E., Kraunus, J., Chen, L. & Baum, C. Retroviral Pseudotransduction for Targeted
984 Cell Manipulation. *Molecular Cell* **16**, 309-315 (2004).
985 https://doi.org:https://doi.org/10.1016/j.molcel.2004.09.023
986 41 Nash, K. L. & Lever, A. M. L. Green fluorescent protein: green cells do not always indicate gene
987 expression. *Gene Therapy* **11**, 882-883 (2004). https://doi.org:10.1038/sj.gt.3302246
988 42 Geering, B., Schmidt-Mende, J., Federzoni, E., Stoeckle, C. & Simon, H.-U. Protein overexpression
989 following lentiviral infection of primary mature neutrophils is due to pseudotransduction. *Journal of*
990 *Immunological Methods* **373**, 209-218 (2011).
991 https://doi.org:https://doi.org/10.1016/j.jim.2011.08.024

992 43 Kim, J. T. *et al.* Dendritic cell–targeted lentiviral vector immunization uses pseudotransduction and
993 DNA-mediated STING and cGAS activation. *Science Immunology* **2**, eaal1329 (2017).
994 https://doi.org:doi:10.1126/sciimmunol.aal1329
995 44 Hung, M. E. & Leonard, J. N. A platform for actively loading cargo RNA to elucidate limiting steps
996 in EV-mediated delivery. *J Extracell Vesicles* **5**, 31027 (2016). https://doi.org:10.3402/jev.v5.31027
997 45 Somiya, M. & Kuroda, S. i. Verification of extracellular vesicle-mediated functional mRNA delivery
998 via RNA editing. *bioRxiv*, 2022.2001.2025.477620 (2022).
999 https://doi.org:10.1101/2022.01.25.477620
1000 46 Yeh, H. W. *et al.* ATP-Independent Bioluminescent Reporter Variants To Improve in Vivo Imaging.
1001 *ACS Chem Biol* **14**, 959-965 (2019). https://doi.org:10.1021/acschembio.9b00150
1002 47 Bäck, S. *et al.* Neuron-Specific Genome Modification in the Adult Rat Brain Using CRISPR-Cas9
1003 Transgenic Rats. *Neuron* **102**, 105-119.e108 (2019).
1004 https://doi.org:https://doi.org/10.1016/j.neuron.2019.01.035
1005 48 Donahue, P. S. *et al.* The COMET toolkit for composing customizable genetic programs in
1006 mammalian cells. *Nature Communications* **11**, 779 (2020). https://doi.org:10.1038/s41467-019-
1007 14147-5
1008 49 Votteler, J. *et al.* Designed proteins induce the formation of nanocage-containing extracellular
1009 vesicles. *Nature* **540**, 292-295 (2016). https://doi.org:10.1038/nature20607
1010 50 Sauer, B. & Henderson, N. Targeted insertion of exogenous DNA into the eukaryotic genome by
1011 the Cre recombinase. *New Biol* **2**, 441-449 (1990).
1012 51 Blessing, D., Déglon, N. & Schneider, B. L. in *Recombinant Protein Expression in Mammalian Cells:*
1013 *Methods and Protocols* (ed David L. Hacker) 259-274 (Springer New York, 2018).
1014 52 Gunnels, T. F., Stranford, D. M., Mitrut, R. E., Kamat, N. P. & Leonard, J. N. Elucidating Design
1015 Principles for Engineering Cell-Derived Vesicles to Inhibit SARS-CoV-2 Infection. *Small* **18**,
1016 2200125 (2022). https://doi.org:https://doi.org/10.1002/smll.202200125
1017 53 Fischer, K. B., Collins, H. K. & Callaway, E. M. Sources of off-target expression from recombinase-
1018 dependent AAV vectors and mitigation with cross-over insensitive ATG-out vectors. *Proceedings of*

1019 *the National Academy of Sciences* **116**, 27001-27010 (2019).
1020 https://doi.org:doi:10.1073/pnas.1915974116
1021 54 Osanai, Y. *et al.* 5′ Transgenes drive leaky expression of 3′ transgenes in Cre-inducible bi-cistronic
1022 vectors. *Molecular Therapy - Methods & Clinical Development* **32**, 101288 (2024).
1023 https://doi.org:https://doi.org/10.1016/j.omtm.2024.101288
1024 55 Gutierrez-Guerrero, A., Cosset, F.-L. & Verhoeyen, E. Lentiviral vector pseudotypes: precious tools
1025 to improve gene modification of hematopoietic cells for research and gene therapy. *Viruses* **12**,
1026 1016 (2020).
1027 56 Dautzenberg, I. J. C., Rabelink, M. J. W. E. & Hoeben, R. C. The stability of envelope-pseudotyped
1028 lentiviral vectors. *Gene Therapy* **28**, 89-104 (2021). https://doi.org:10.1038/s41434-020-00193-y
1029 57 Ma, D. *et al.* Engineered extracellular vesicles enable high-efficient delivery of intracellular
1030 therapeutic proteins. *Protein & Cell* **15**, 724-743 (2024). https://doi.org:10.1093/procel/pwae015
1031 58 Meyer, C. *et al.* Pseudotyping exosomes for enhanced protein delivery in mammalian cells. *Int J*
1032 *Nanomedicine* **12**, 3153-3170 (2017). https://doi.org:10.2147/ijn.S133430
1033 59 Kim, I. S. *et al.* Mechanism of membrane fusion induced by vesicular stomatitis virus G protein.
1034 *Proceedings of the National Academy of Sciences* **114**, E28-E36 (2017).
1035 https://doi.org:doi:10.1073/pnas.1618883114
1036 60 Wang, J. *et al.* Highly efficient homology-driven genome editing in human T cells by combining zinc-
1037 finger nuclease mRNA and AAV6 donor delivery. *Nucleic Acids Research* **44**, e30-e30 (2015).
1038 https://doi.org:10.1093/nar/gkv1121
1039 61 Ellis, B. L. *et al.* A survey of ex vivo/in vitro transduction efficiency of mammalian primary cells and
1040 cell lines with Nine natural adeno-associated virus (AAV1-9) and one engineered adeno-associated
1041 virus serotype. *Virology Journal* **10**, 74 (2013). https://doi.org:10.1186/1743-422X-10-74
1042 62 Gutierrez-Guerrero, A., Cosset, F. L. & Verhoeyen, E. Lentiviral Vector Pseudotypes: Precious Tools
1043 to Improve Gene Modification of Hematopoietic Cells for Research and Gene Therapy. *Viruses* **12**
1044 (2020). https://doi.org:10.3390/v12091016

1045 63 Fredericksen, B. L. & Whitt, M. A. Vesicular stomatitis virus glycoprotein mutations that affect
1046 membrane fusion activity and abolish virus infectivity. *Journal of Virology* **69**, 1435-1443 (1995).
1047 https://doi.org:10.1128/jvi.69.3.1435-1443.1995
1048 64 Liang, X. *et al.* Engineering of extracellular vesicles for efficient intracellular delivery of multimodal
1049 therapeutics including genome editors. *Nature Communications* **16**, 4028 (2025).
1050 https://doi.org:10.1038/s41467-025-59377-y
1051 65 Nikolic, J. *et al.* Structural basis for the recognition of LDL-receptor family members by VSV
1052 glycoprotein. *Nature communications* **9**, 1029 (2018).
1053 66 Dobson, C. S. *et al.* Antigen identification and high-throughput interaction mapping by
1054 reprogramming viral entry. *Nature Methods* **19**, 449-460 (2022). https://doi.org:10.1038/s41592-
1055 022-01436-z
1056 67 Gao, Y. & Bergman, I. Vesicular Stomatitis Virus (VSV) G Glycoprotein Can Be Modified to Create
1057 a Her2/Neu-Targeted VSV That Eliminates Large Implanted Mammary Tumors. *Journal of Virology*
1058 **97**, e00372-00323 (2023). https://doi.org:10.1128/jvi.00372-23
1059 68 Issa, S. S., Shaimardanova, A. A., Solovyeva, V. V. & Rizvanov, A. A. Various AAV Serotypes and
1060 Their Applications in Gene Therapy: An Overview. *Cells* **12** (2023).
1061 https://doi.org:10.3390/cells12050785
1062 69 Maguire, C. A. *et al.* Microvesicle-associated AAV Vector as a Novel Gene Delivery System.
1063 *Molecular Therapy* **20**, 960-971 (2012). https://doi.org:https://doi.org/10.1038/mt.2011.303
1064 70 Kovács, O. T. *et al.* Impact of Medium-Sized Extracellular Vesicles on the Transduction Efficiency
1065 of Adeno-Associated Viruses in Neuronal and Primary Astrocyte Cell Cultures. *Int J Mol Sci* **22**
1066 (2021). https://doi.org:10.3390/ijms22084221
1067 71 Sonntag, F., Bleker, S., Leuchs, B., Fischer, R. & Kleinschmidt Jürgen, A. Adeno-Associated Virus
1068 Type 2 Capsids with Externalized VP1/VP2 Trafficking Domains Are Generated prior to Passage
1069 through the Cytoplasm and Are Maintained until Uncoating Occurs in the Nucleus. *Journal of*
1070 *Virology* **80**, 11040-11054 (2006). https://doi.org:10.1128/jvi.01056-06

1071 72 Bentler, M. *et al.* Modifying immune responses to adeno-associated virus vectors by capsid
1072 engineering. *Molecular Therapy - Methods & Clinical Development* **30**, 576-592 (2023).
1073 https://doi.org:https://doi.org/10.1016/j.omtm.2023.08.015
1074 73 Nisanov, A. M., de Jesús, J. A. R. & Schaffer, D. V. Advances in AAV capsid engineering: Integrating
1075 rational design, directed evolution and machine learning. *Molecular Therapy* **33**, 1937-1945 (2025).
1076 74 Stranford, D. M., Hung, M. E., Gargus, E. S., Shah, R. N. & Leonard, J. N. A Systematic Evaluation
1077 of Factors Affecting Extracellular Vesicle Uptake by Breast Cancer Cells. *Tissue Eng Part A* **23**,
1078 1274-1282 (2017). https://doi.org:10.1089/ten.TEA.2017.0158
1079 75 Welsh, J. A. *et al.* Minimal information for studies of extracellular vesicles (MISEV2023): From basic
1080 to advanced approaches. *Journal of Extracellular Vesicles* **13**, e12404 (2024).
1081 https://doi.org:https://doi.org/10.1002/jev2.12404
1082 76 von Lersner, A. K. *et al.* Multiparametric Single-Vesicle Flow Cytometry Resolves Extracellular
1083 Vesicle Heterogeneity and Reveals Selective Regulation of Biogenesis and Cargo Distribution.
1084 *ACS Nano* **18**, 10464-10484 (2024). https://doi.org:10.1021/acsnano.3c11561
1085 77 Sork, H. *et al.* Heterogeneity and interplay of the extracellular vesicle small RNA transcriptome and
1086 proteome. *Scientific Reports* **8**, 10813 (2018). https://doi.org:10.1038/s41598-018-28485-9
1087 78 Kim, H., Kim, M., Im, S. K. & Fang, S. Mouse Cre-LoxP system: general principles to determine
1088 tissue-specific roles of target genes. *Lab Anim Res* **34**, 147-159 (2018).
1089 https://doi.org:10.5625/lar.2018.34.4.147

1090

1091

1092 **FIGURES**

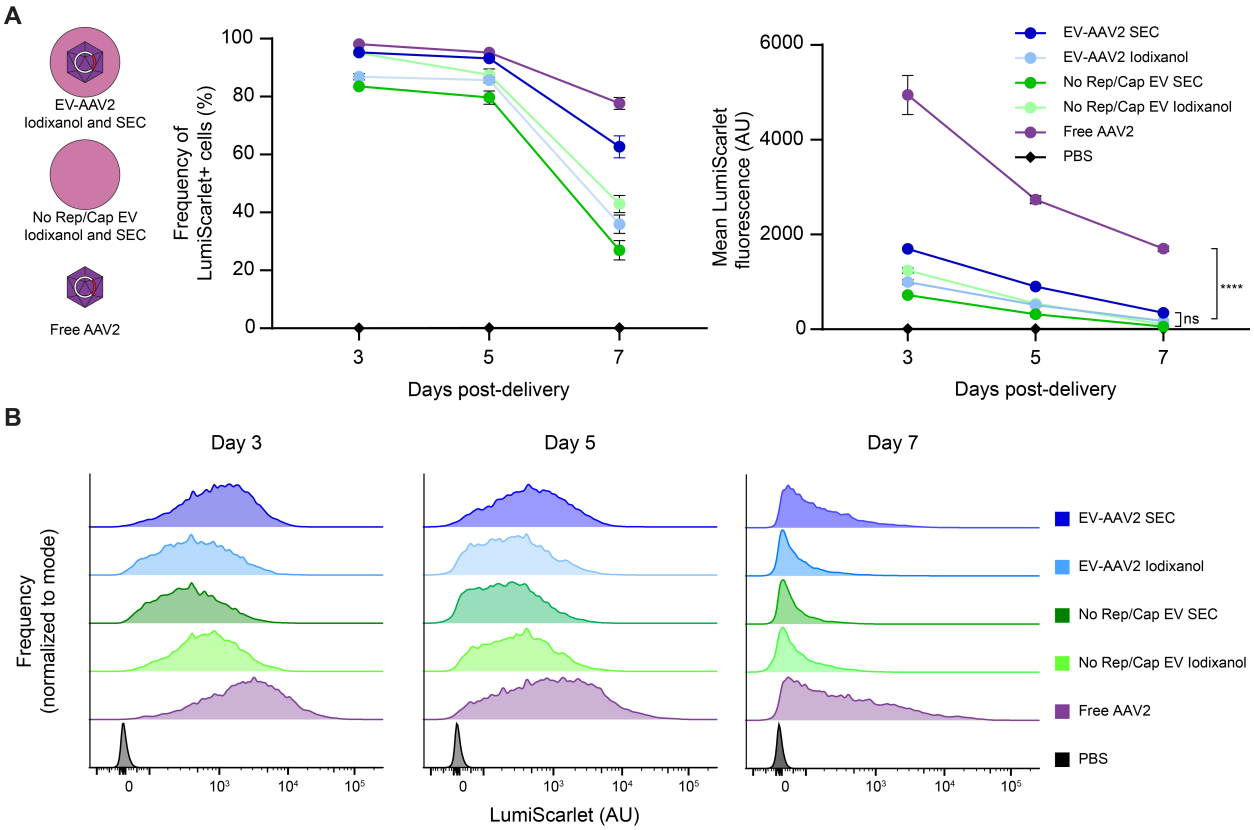

1093

1094 Figure 1

1095

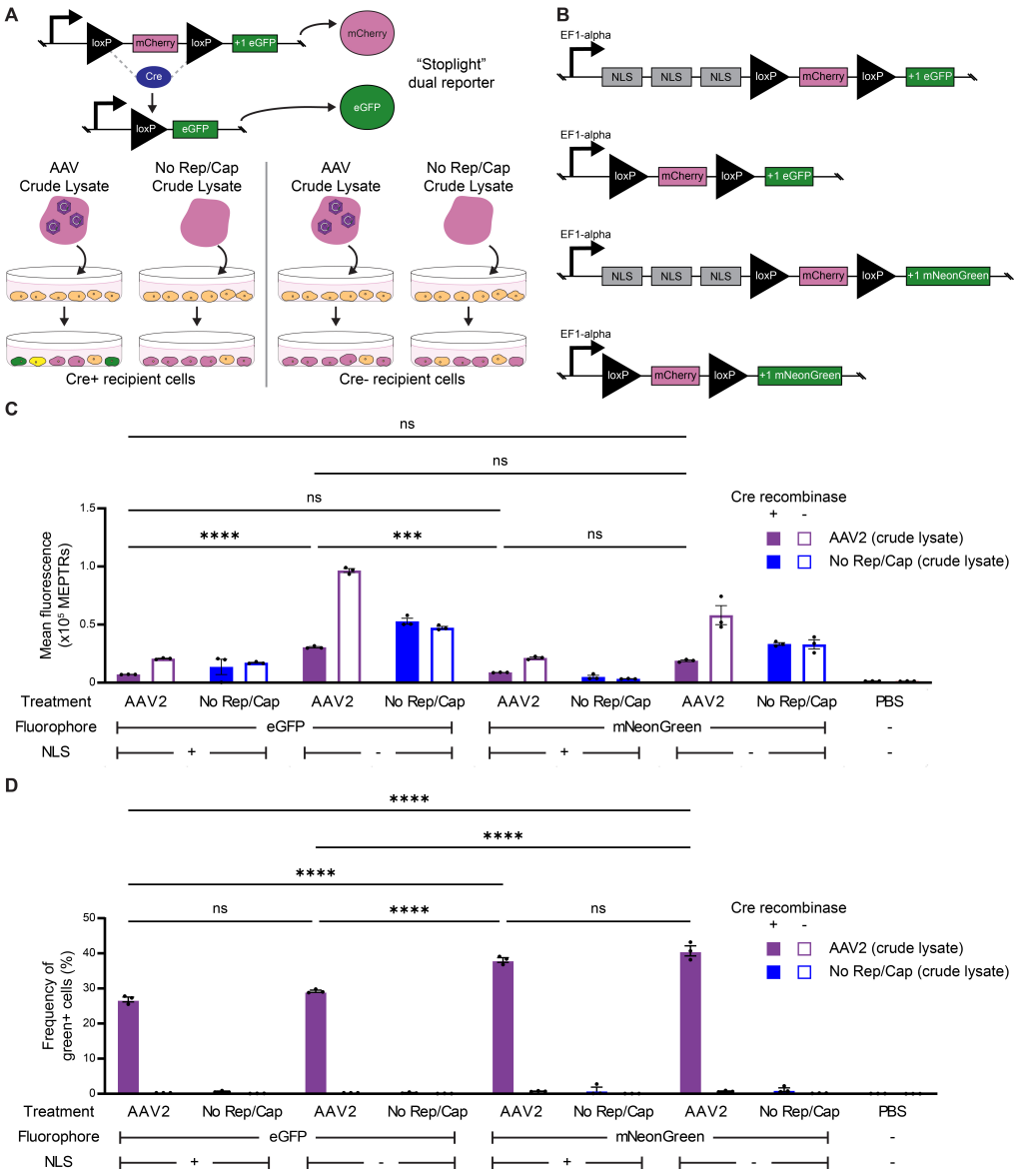
A
loxP
mCherry
loxP
+1 eGFP
Cre
mCherry
eGFP
"Stoplight" dual reporter
AAV Crude Lysate
No Rep/Cap Crude Lysate
Cre+ recipient cells
Cre- recipient cells
B
EF1-alpha
NLS
+1 mNeonGreen
C
Mean fluorescence (x10^5 MEPTRs)
Cre recombinase
AAV2 (crude lysate)
No Rep/Cap (crude lysate)
ns
****
***
Treatment
Fluorophore
NLS
AAV2
No Rep/Cap
PBS
eGFP
mNeonGreen
D
Frequency of green+ cells (%)

Figure 2

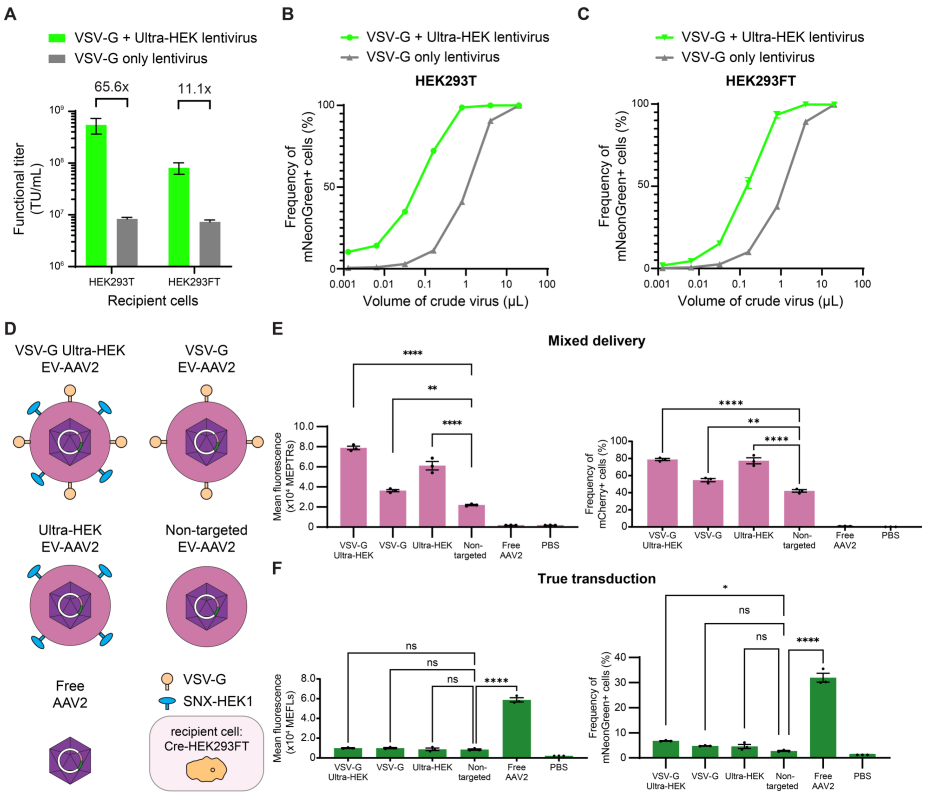
A
VSV-G + Ultra-HEK lentivirus
VSV-G only lentivirus
65.6x
11.1x
Functional titer (TU/mL)
HEK293T
HEK293FT
Recipient cells
B
HEK293T
Frequency of mNeonGreen+ cells (%)
Volume of crude virus (µL)
C
HEK293FT
D
VSV-G Ultra-HEK EV-AAV2
VSV-G EV-AAV2
Ultra-HEK EV-AAV2
Non-targeted EV-AAV2
Free AAV2
VSV-G
SNX-HEK1
recipient cell: Cre-HEK293FT
E
Mixed delivery
Mean fluorescence (X10⁴ MEFTRs)
Frequency of mCherry+ cells (%)
VSV-G Ultra-HEK
VSV-G
Ultra-HEK
Non-targeted
Free AAV2
PBS
F
True transduction
Mean fluorescence (X10⁴ MEFLs)
Frequency of mNeonGreen+ cells (%)

Figure 3

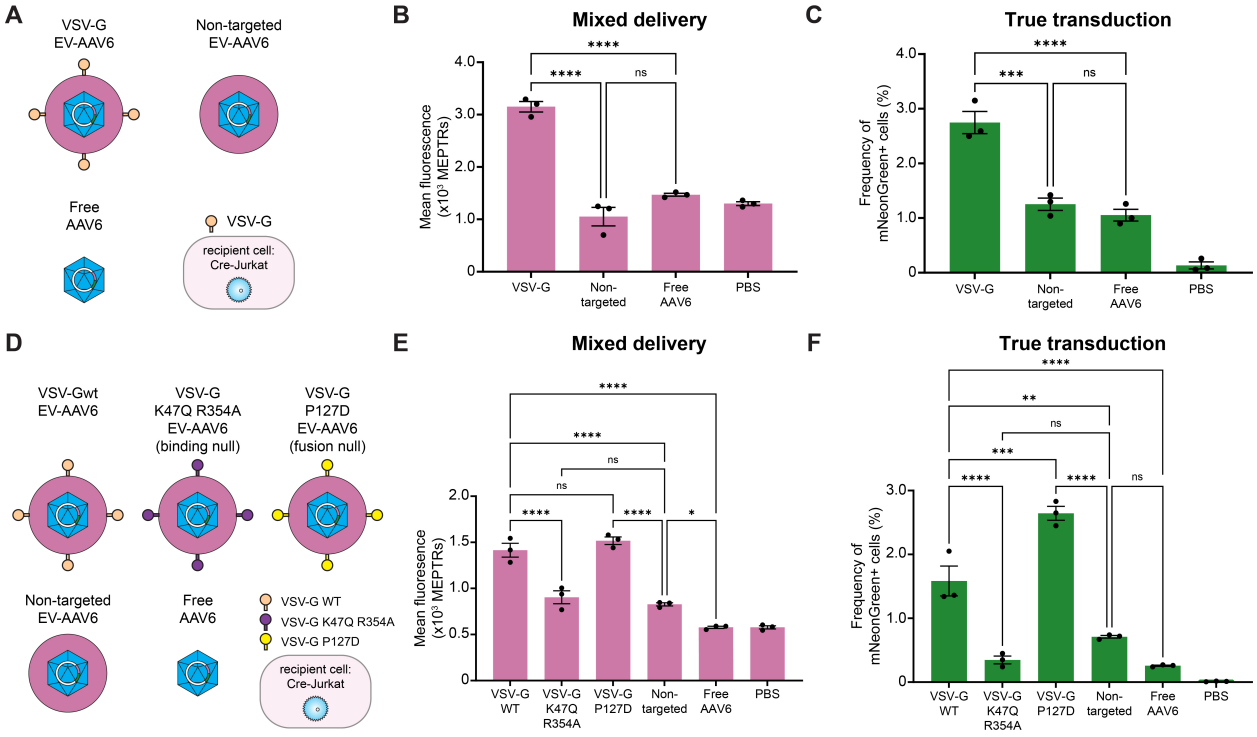

Figure 4

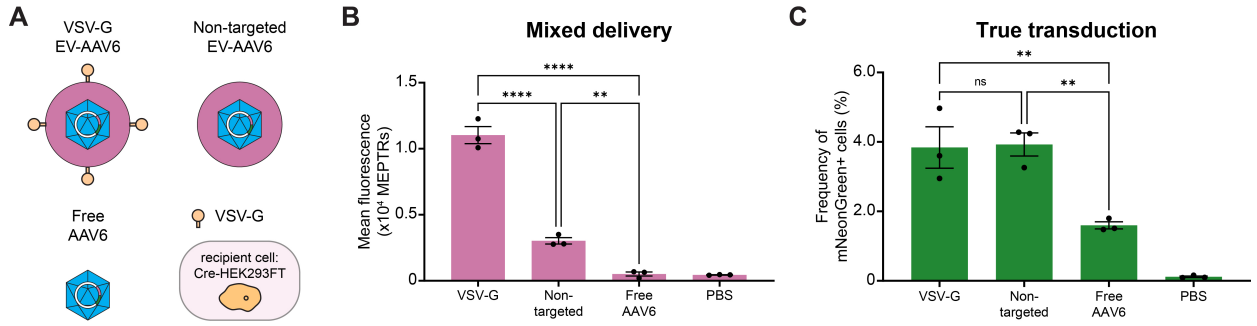

Figure 5

1109 **FIGURE CAPTIONS**

1110 **Figure 1: EV-AAV pseudotransduction complicates distinguishing true transduction. (A)** EV-AAV-
1111 mediated protein delivery, mRNA and/or expression in HEK293FT recipient cells. Vector compositions and
1112 EV-AAV purification methods employed to separate EVs and free AAV are summarized in cartoons at left.
1113 Free AAV (which should confer minimal pseudotransduction) conferred significantly greater fluorescence
1114 than did EV-AAV controls. EV-AAV vectors were generally similar to the No Rep/Cap (protein delivery only)
1115 control at all time points post-delivery. **(B)** Representative histograms of LumiScarlet fluorescence from
1116 samples reported in (A). No subpopulations are apparent that can rigorously distinguish protein delivery
1117 from transduction. Experiments were performed in biological triplicate. Data shown are from one of two
1118 independent experiments (second experiment: **Figures S8**,**9**). Error bars indicate standard error of the
1119 mean. Multicomparison statistical analysis was performed using a two-way ANOVA test, followed by Tukey's
1120 multiple comparison test to evaluate specific comparisons (****$p < 0.0001$). ns; not significant; PBS:
1121 phosphate-buffered saline; SEC: size exclusion chromatography.

1122

1123 **Figure 2: A Cre recombinase-based dual reporter system distinguishes mixed delivery and**
1124 **transduction. (A)** Schematic depicting the expected function of the stoplight dual-reporter system in which
1125 Cre expressed in recipient cells acts upon incoming AAV genomes to switch them from expression of a red
1126 reporter to a green reporter. Free AAV mediates transduction only (green); EV-AAV mediates both mixed
1127 delivery (red) and transduction (green) and sometimes both (yellow); No Rep/Cap EVs can only mediate
1128 mixed delivery (red). **(B)** Cre-responsive plasmids evaluated in this experiment. **(C,D)** Mixed delivery (C)
1129 and transduction (D) conferred by various vector compositions. Note: some mCherry gene expression could
1130 occur in recipient cells prior to Cre-mediated recombination (or in the possible absence of recombination),
1131 such that (C) includes both mixed delivery and this ambiguous de novo gene expression. Samples were
1132 normalized to include 1e9 vector genomes per well (for AAV crude lysate conditions) or a volume-equivalent
1133 of the AAV2 crude lysate condition for No Rep/Cap crude lysate conditions (10^4 recipient cells). Experiments
1134 were performed in biological triplicate. One of two independent experiments is shown (second experiment:
1135 **Figure S10**). Error bars indicate standard error of the mean. Multicomparison statistical analysis was
1136 performed using a two-way ANOVA test, followed by Tukey's multiple comparison test to evaluate specific

1137 comparisons (*$p < 0.05$, **$p < 0.01$, ***$p < 0.001$, ****$p < 0.0001$). NLS: nuclear localization sequence; ns:
1138 not significant; PBS: phosphate-buffered saline.
1139
1140 **Figure 3: EV-AAV2 functionalization increases mixed delivery but not transduction of HEK293FTs.**
1141 **(A-C)** Validation of Ultra-HEK (Syenex) for enhancing lentiviral delivery to HEK293T and HEK293FT cells.
1142 Relative fold-improvements in functional titer compared to a standard VSV-G-pseudotyped lentiviral vector
1143 are indicated. (**D**) Schematic depicting vectors used in (E,F) (Cre-HEK293FT recipient cells). (**E,F**) Mixed
1144 delivery quantified by mean fluorescence in MEPTRs (left) and frequency of mCherry positive cells (right)
1145 (E) and transduction quantified by mean fluorescence in MEFLs (left) and frequency of mNeonGreen
1146 positive cells (right) (F) to HEK293FT cells (5 days post-delivery). Samples were normalized to include 1e9
1147 vector genomes per well for each condition (10^4 recipient cells). VSV-G and Ultra-HEK-functionalized EV-
1148 AAV increase mixed delivery but only modestly increase transduction and only when combined.
1149 Experiments were performed in biological triplicate. One of two independent experiments is shown (second
1150 experiment: **Figure S15**). Error bars indicate standard error of the mean. Multicomparison statistical
1151 analysis was performed using a one-way ANOVA test, followed by Tukey's multiple comparison test to
1152 evaluate specific comparisons (*$p < 0.05$, **$p < 0.01$, ***$p < 0.001$, ****$p < 0.0001$). PBS: phosphate-
1153 buffered saline.
1154
1155 **Figure 4: VSV-G functionalization of EV-AAV6 increases transduction and mixed delivery to Jurkat**
1156 **T cells by increasing uptake. (A)** Schematic depicting vectors used in (B,C) (Cre-Jurkat T cell recipient
1157 cells). (**B,C**) Mixed delivery (B) and transduction (C) in Jurkat T cells (5 days post-delivery). Samples were
1158 normalized to include 1e9 vector genomes per well for each condition (10^4 recipient cells). VSV-G
1159 functionalization significantly increases mixed delivery to and transduction of Jurkats. **(D)** Schematic
1160 depicting vectors used in (E,F) (Cre-Jurkat T cell recipient cells). (**E,F**) Mixed delivery (E) and transduction
1161 (F) in Jurkat T cells (5 days post-delivery). Samples were normalized to include 2e9 vector genomes per
1162 condition (10^4 recipient cells). VSV-G functionalization significantly increases mixed delivery and
1163 transduction of Jurkats. Mixed delivery and transduction are increased only by enhanced binding of
1164 recipient cells (VSV-G WT and VSV-G P127D vectors). Experiments were performed in biological triplicate.

1165 Data shown are from one of two independent experiments (second experiments in **Figure S18**). Error bars
1166 indicate standard error of the mean. Multicomparison statistical analysis was performed using a one-way
1167 ANOVA test, followed by Tukey's multiple comparison test to evaluate specific comparisons (*$p < 0.05$,
1168 **$p < 0.01$, ***$p < 0.001$, ****$p < 0.0001$). PBS: phosphate-buffered saline.
1169
1170 **Figure 5: Determinants of EV-AAV delivery to HEK293FT cells apply across two AAV serotypes. (A)**
1171 Schematic depicting vectors used in (B,C) (Cre-HEK293FT recipient cells). (**B,C**) Mixed delivery (B) and
1172 transduction (C) to HEK29FT cells (5 days post-delivery). Samples were normalized to include 1e9 vector
1173 genomes per well for each condition (10^4 recipient cells). VSV-G functionalization enhances mixed delivery
1174 but not transduction by EV-AAV6, concordant with observations made using EV-AAV2. Experiments were
1175 performed in biological triplicate. One of two independent experiments is shown (second experiment:
1176 **Figure S20**). Error bars indicate standard error of the mean. Multicomparison statistical analysis was
1177 performed using a one-way ANOVA test, followed by Tukey's multiple comparison test to evaluate specific
1178 comparisons (*$p < 0.05$, **$p < 0.01$, ***$p < 0.001$, ****$p < 0.0001$). PBS: phosphate-buffered saline.
1179